

Deep-sea stylasterid $\delta^{18}\text{O}$ and $\delta^{13}\text{C}$ maps inform sampling scheme for paleotemperature reconstructions

Theresa M. King¹, Brad E. Rosenheim¹, and Noel P. James²

5 ¹College of Marine Science, University of South Florida, St. Petersburg, 33701, USA

²Department of Geological Sciences and Geological Engineering, Queens University, Kingston, K7L 3N6, Canada

Correspondence to: Theresa M. King (theresaking@usf.edu)

Abstract. Deep-sea corals have the potential to provide high-resolution paleotemperature records to evaluate oceanographic changes in settings that are vulnerable to current and future ocean warming. The isotopic records preserved in coral skeletal carbonate, however, are limited by their large offsets from isotopic equilibrium with seawater. These “vital effects” are the result of biological influences (kinetic and metabolic) on the calcification of coral skeletons and are well known to drive oxygen and carbon stable isotope ratios ($\delta^{18}\text{O}$ and $\delta^{13}\text{C}$, respectively) away from isotopic equilibrium with environmental variables. In this study, two calcitic stylasterid corals (*Errina fissurata*) are sampled via cross sections through their primary growth axes to create skeletal $\delta^{18}\text{O}$ and $\delta^{13}\text{C}$ maps. The maps reveal a consistent trend of increasing isotopic values toward the innermost portion of the cross sections, with minimal spatial change in carbonate mineralogy; the average center values being ~ 1 ‰ and ~ 3 ‰ closer to seawater $\delta^{18}\text{O}$ and $\delta^{13}\text{C}$ equilibrium values (respectively). We investigate possible mechanisms for these isotopic trends, including potential growth patterns that would drive spatial isotopic trends. Our results highlight the diversity of the stylasterid coral family and because of our unique sampling strategy, we can prescribe that *E. fissurata* corals with minimal mineralogical variability be sampled from the center portions of their stems to achieve accurate paleotemperature reconstructions.

1 Introduction

Robust paleoceanographic temperature proxies are fundamental to understanding past climate changes and sensitivities. Foundational work developed the theory and application of the oxygen isotope paleothermometer in marine biogenic carbonates including foraminiferal tests and shallow water corals (Urey, 1947; McCrea, 1950; Epstein et al., 1953; Emiliani, 1955; Shackleton, 1967; Emiliani et al., 1978). All archives have limits in geographic distribution despite their ability to lengthen the time domain of paleoceanographic records. On the Antarctic margin, for instance, foraminifera are not widely present in marine sediment cores. Scleractinian zooxanthellate corals are limited to lower latitudes. Deep-sea azooxanthellate corals have been used to elucidate ocean history on different time scales (Adkins et al., 1998; Robinson et al., 2005; Robinson and van de Flierdt, 2009; Burke and Robinson, 2012; Chen et al., 2020), but normally the extraction of continuous records

30 from individual colonies has been precluded by the complexity of growth habit and the fidelity of elemental and isotopic records archived in their skeletons (Weber, 1973; Wisshak et al., 2009; Robinson et al., 2014). Corals can incorporate high resolution geochemical records over decades to millennia while remaining fixed to the seafloor; this is especially useful to observe regional and global processes causing ocean water masses to heave and shoal at timescales over which the coral is alive (Andrews et al., 2002; Druffel et al., 1990; Druffel, 1997; Griffin and Druffel, 1989; Risk et al., 2002). Such archives are
35 crucial for paleotemperature reconstructions.

Biom mineralization of carbonate coral skeletons records both environmental information and biological effects (also known as “vital effects”). The latter must be understood to obtain high-fidelity records of ocean change. Vital effects can obscure environmental information stored in skeletal records, such as oxygen and carbon stable isotope ratios ($\delta^{18}\text{O}$ and $\delta^{13}\text{C}$, respectively). Slow rates of biological calcification allow for carbon and oxygen isotopes of carbonate minerals to approach
40 isotopic equilibrium with seawater, a state governed by thermodynamics (Swart, 1983). Biological calcification, however, also includes nonequilibrium fractionation which cannot be interpreted directly as environmental signal (Weber and Woodhead, 1970; McConnaughey, 1989a). Early research on corals demonstrated that isotopic variability can be caused by metabolic fractionation, kinetic fractionation, or a combination of both (McConnaughey, 1989a). The metabolic fractionation is characterized by a change in carbon isotope composition of the dissolved inorganic carbon pool from which the coral calcifies
45 via incorporation of the products of respiration and photosynthesis of algal symbionts or respiration of the coral itself (Swart, 1983; McConnaughey, 1989a). The kinetic fractionation is described as a product of the kinetic isotope effect: discrimination against heavy oxygen and carbon isotopes during hydration and hydroxylation of CO_2 during biomineralization (McConnaughey, 1989b). Rapid calcification results in greater disequilibrium of skeletal $\delta^{18}\text{O}$ and $\delta^{13}\text{C}$ as the CO_2 does not have sufficient time to equilibrate with ambient seawater before being incorporated into the skeleton (McConnaughey, 1989b).

50 Vital effects have been invoked to explain skeletal $\delta^{18}\text{O}$ and $\delta^{13}\text{C}$ values lower than equilibrium, and the strong linear relationship between $\delta^{18}\text{O}$ and $\delta^{13}\text{C}$ values has been used to further understand vital effects exhibited by corals from varied ocean depths and latitudes (Smith et al., 2000; Emiliani et al., 1978; Heikoop et al., 2000; Mikkelsen et al., 2008; McConnaughey, 1989a). Early work by Emiliani et al. (1978) examined the $\delta^{18}\text{O}$ and $\delta^{13}\text{C}$ recorded by a solitary scleractinian coral (class Hexacorallia, order Scleractinia) and found that both isotopic ratios trended toward higher values from the bottom
55 to top of the coral. This was interpreted as a slowing growth rate with time, approaching isotopic equilibrium with the surrounding seawater (Emiliani et al., 1978). Additional work on solitary scleractinians by Adkins et al. (2003) employed a microsampling approach for $\delta^{18}\text{O}$ and $\delta^{13}\text{C}$ that identified new mechanisms for vital effects. Along with the lowest isotopic values occurring at regions of rapid calcification, Adkins et al. (2003) observed a break in the linear relationship of stable isotopic ratios in these regions. The authors hypothesized that rapid biomineralization drives the internal calcifying fluid pH
60 toward higher values, increasing the pumping of CO_2 inward, which results in opposite effects on the carbon and oxygen isotope composition in the skeleton by stabilizing fractionation of carbon isotopes increasing fractionation of oxygen isotopes

due to pH driven changes in carbonate speciation (Adkins et al., 2003). Later work on bamboo corals (class Octocorallia, order Malacalcyonacea) sampled across and along their vertical growth axes resulted in low $\delta^{18}\text{O}$ and $\delta^{13}\text{C}$ values near the innermost portion of the coral and at the distal tips (Hill et al., 2011). Interpreting the lower isotope ratios, however, was complicated because the assumed faster calcification rates in these regions were not supported by calculated growth rates, and the locations of maximum growth rates were not consistent for a single specimen (Hill et al., 2011). A further understanding of vital effects was established by Chen et al. (2018) who investigated the role of the carbonic anhydrase enzyme which catalyzes the hydration and hydroxylation of CO_2 . The authors determined that the amount of the enzyme in the calcifying fluid determines the internal speciation of carbonate and thus, alters the slope of the linear $\delta^{18}\text{O}$ and $\delta^{13}\text{C}$ relationship (Chen et al., 2018).

The need for accurate paleotemperature archives underscores the need to understand the impact of vital effects on deep-sea corals. Stylasterid corals (class Hydrozoa, order Anthoathecata) are a ubiquitous taxon of deep-sea corals that occupy ocean depths from the surface to greater than 2700 m, and can be found in high and low latitudes, having great potential for paleoceanographic reconstructions (Cairns, 2011). Stylasterid geochemical work has expanded over the last several years, but because of the inherent diversity of this coral family, research is still needed to understand vital effect-induced isotope fractionation. Early work by Weber and Woodhead (1972) demonstrated that shallow water stylasterids (genus *Distichopora* and *Stylaster*) had precipitated their skeletons closer to isotopic equilibrium than some scleractinian corals. Later work by both Wisshak et al. (2009) and Black and Andrus (2012) examined possible diagenetic effects on the stable isotopic geochemistry of *Errina dabneyi* and *Stylaster erubescens*, respectively. More recently, Samperiz et al. (2020) have produced a compilation of stylasterid skeletal $\delta^{18}\text{O}$ and $\delta^{13}\text{C}$ records from nearly 100 specimens. Similar to the deep-sea scleractinian corals, Samperiz et al. (2020) found the lowest $\delta^{18}\text{O}$ and $\delta^{13}\text{C}$ values in the innermost portion of the main coral trunk and at the distal growth tips, supporting rapid growth in those regions. This work also found that skeletal mineralogy influences $\delta^{18}\text{O}$ and $\delta^{13}\text{C}$ values, whereby calcitic stylasterids record slightly lower values than their aragonitic counterparts (Samperiz et al., 2020). Stylasterid carbonate skeletons can consist of aragonite, calcite, or a mixture of both polymorphs (Cairns and Macintyre, 1992; Kershaw et al., 2023). Another characteristic thus far unique to stylasterids is the absence of pH upregulation within the calcifying fluid (Stewart et al., 2022). The analysis of boron isotopes from calcitic, aragonitic, and mixed stylasterids (*Errina* spp and *Stylaster* spp) compared to those of scleractinian corals support a completely different calcification method wherein stylasterids do not elevate internal pH to promote calcification (Stewart et al., 2022). A largely unknown calcification strategy, paired with variable mineralogy that could impact stable isotopic records highlight a need to develop a deeper understanding of these corals so that we may accurately reconstruct paleoceanographic conditions.

Here we establish a link between isotopic changes and growth pattern of a deep-sea stylasterid using two *Errina fissurata* specimens. We generate $\delta^{18}\text{O}$ and $\delta^{13}\text{C}$ maps over coral surfaces perpendicular to and along vertical growth axes to evaluate the locations and magnitudes of isotopic variability. We compare our skeletal maps to calculated seawater equilibrium values, mineralogical data, and isotopic trends modelled from hypothesized coral growth scenarios to determine the influences on

$\delta^{18}\text{O}$ and $\delta^{13}\text{C}$ and potential implications for paleoceanographic reconstructions. Contradictory to previous research, the isotopic values most representative of environmental signals in these corals are recorded in the innermost portion of the coral stems. Ultimately, we prescribe targeted sampling rather than bulk drilling methods for the most accurate paleotemperature reconstructions for *E. fissurata*.

2 Methods

2.1 Study location and specimen collection

The Ross Sea is a region of bottom water formation for the world's oceans, a characteristic that influences the local oceanography in which the stylasterids live. The region experiences seasonal katabatic winds that create sea ice-forming polynyas, which in turn, create High Salinity Shelf Water through the process of brine rejection (Kurtz and Bromwich, 1985; Picco et al., 2000). The High Salinity Shelf Water flows along the western Ross Sea and out to the shelf edge where it mixes with upwelled modified Circumpolar Deep Water, resulting in a component of dense Antarctic Bottom Water that spills down the continental slope (Gordon et al., 2009; Jacobs et al., 1970; Sandrini et al., 2007).

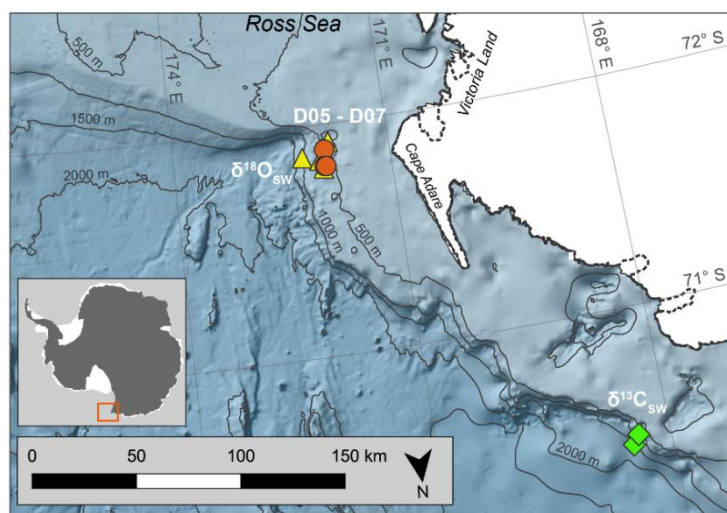


Figure 1: Map of coral collection sites. D05–D07 represent dredge sites during NBP07-01 from which coral samples were collected on the outer western Ross Sea continental shelf. The diamonds and triangles mark the stations used to calculate the seawater isotopic ratios ($\delta^{13}\text{C}_{\text{sw}}$ and $\delta^{18}\text{O}_{\text{sw}}$; Table S2; Fig. S2). Antarctic landmass and ice sheets are colored white (Gerrish et al., 2022) with the coastline marked by a solid black line, and ice sheet grounding line denoted by a dotted black line (Mouginot et al., 2017). Bathymetric contours are in increments of 500 m (Arndt et al., 2013). Antarctic inset denotes sampling site marked by red box. Map was created using the Quantarctica data set collection within QGIS (Matsuoka et al., 2021).

The stylasterid coral specimens for this study were collected aboard the U.S. Antarctic Program expedition NBP07-01 near Cape Adare in the western Ross Sea. Seamounts on the outer continental shelf were dredged at a water depth ranging 400 m

to 600 m and the corals used here were from the fifth through seventh dredges (D05–D07; Fig. 1, Table 1). The recovered stylasterid corals were predominantly *Errina* spp. and specimens were recovered both alive and dead (as evidenced by their pigmentation), some with growth tips intact. For this study, one live-collected and one dead-collected stylasterid were selected for isotopic analyses (EA-11 and EA-12, respectively), targeting the longest whole specimens ranging from ~9 to 10 cm long (Fig. 2). Additional coral specimens were identified to the species level as *Errina fissurata* based on descriptions of morphological characteristics (see Cairns, 1983a, b, 1991) that were identified using scanning electron microscopy (SEM). The corals used for identification, EA-20 and EA-21, were sputter-coated in gold palladium and not suitable for geochemical analysis. Additional specimens EA-22 through EA-24 were also imaged using SEM for physical evidence of diagenesis (e.g., Wisshak et al., 2009; see section 4.2.2).

2.2 Coral sampling and isotope analysis

The stylasterid specimens were sampled for stable oxygen and carbon isotope measurements ($\delta^{18}\text{O}$ and $\delta^{13}\text{C}$, respectively) over cross sections of their major growth axes. A Gryphon diamond band saw was used to slice discs measuring approximately 2–3 mm thick from each specimen’s main stems (three from EA-11 and two from EA-12; Fig. 2). Additionally, a longer 8 mm thick section was cut from the lower main stem of EA-11 (EA-11d; Fig. 2). This cylindrical main stem section was sliced in half lengthwise with the band saw and sampled along the vertical face. Each coral disc was sonicated in 18.2 megohm deionized (DI) water until no remaining loose particles were released then dried in a 50° C oven for 24 hours. The coral discs were then drilled over their surfaces with a New Wave MicroMill system at grid spacing that varied between 1 and 1.5 mm, based on the diameter of the slice and ampullae in the disc. The MicroMill was configured with a 0.5 mm round carbide bur for each hole that plunged to a maximum depth of 1 mm, just far enough to obtain enough carbonate material for analysis (~80–120 μg CaCO_3). The carbonate powder from each hole was transferred to vials and the sample hole and stylasterid surface were cleaned with compressed air or nitrogen to remove any residual powder between drilling intervals.

Lat. (°S)	Long. (°E)	Water Depth (m)	Dredge	Temp. at Depth (°C)	$\delta^{18}\text{O}$ seawater (‰, SMOW)	$\delta^{13}\text{C}$ seawater (‰, PDB)
71.89	171.9	490-593	D05	-0.10 ± 0.09	-0.26 ± 0.06	0.66 ± 0.05
71.82	171.92	518-643	D06			
71.82	171.9	489-599	D07			

Table 1: Sample collection data including approximate coordinates of dredges, the range of water depths sampled, names of each dredge, and approximate seawater properties. Temperature is averaged for dredge depth range using measurements from nearby AnSlope stations (Visbeck, 2015; Jacobs, 2015; Gordon, 2016). The corresponding potential temperatures and salinities for this depth range were used to determine the $\delta^{18}\text{O}$ of the seawater based on values reported by Jacobs et al. (1985) for Antarctic margin water masses. The seawater $\delta^{13}\text{C}$ is an average of values reported for the same depth range from nearby World Ocean Circulation Experiment stations (WOCE, 2002; Fig. S1).

The sample vials were flushed with helium and acidified with phosphoric acid at 50° C to generate CO₂ that was analyzed at the University of South Florida College of Marine Science using a Thermo Scientific MAT 253 stable isotope ratio mass spectrometer with a Gas Bench II preparatory device. All reported values are in standard delta (δ) notation and reported as per mil (‰, relative to PDB). Laboratory reference materials Borba (δ¹³C: 2.89 ‰, δ¹⁸O: -6.15 ‰), TSF-1 (δ¹³C: 1.95 ‰, δ¹⁸O: -2.20 ‰), and Leco (δ¹³C: -15.44 ‰, δ¹⁸O: -20.68 ‰), were used for instrument correction and normalizing to the Pee Dee Belemnite scale (PDB), and an internal Antarctic coral standard was used for quality control. To account for fractionation of oxygen isotopes during acidification (Kim et al., 2007) we measured calcite reference materials, which corrected for fractionation during the transfer onto the PDB scale. The analytical uncertainty (1σ) of the MAT 253 during this study was ±0.083 ‰ δ¹³C and ±0.064 ‰ δ¹⁸O.



155

Figure 2: Whole coral specimens EA-11 (left) and EA-12 (right). EA-11 was live-collected, and EA-12 was dead. Sample discs are labelled, and the corresponding isotope maps are in Fig. 3.

2.3 Mineralogical analysis

Coral slices EA-11b and EA-11d were analyzed for mineralogy using X-ray diffraction (XRD) after being sampled for stable isotopic analyses. The XRD diffraction patterns were obtained on a Bruker D8 Advance Powder Diffractometer with Lynxeye detector and motorized slits assembly at the University of South Florida X-ray Diffraction Facility and Solid State Characterization Core Laboratory. The EA-11b samples were drilled from the pink and white regions of the slice using the MicroMill and incorporated skeletal material from regions that include the spots used for isotopic analysis (Fig. S3). Detailed mineralogy for EA-11b was determined by analyzing between 24.0–35.5 2θ using copper tube radiation. The flat surface of EA-11d was not pulverized, but rather scanned to isolate each axially oriented color band (two pink bands on the outsides of the section, and a white band on the inside (Fig. 2, section d in EA-11, and Fig. S3). The EA-11d coral slice was centred within a beam of very small divergence, 0.02°, that was able to analyse a single band of color at a time. The crystalline phases were identified with Bruker-EVA 7 software and the Crystallographic Open Database (COD).

165

3 Results

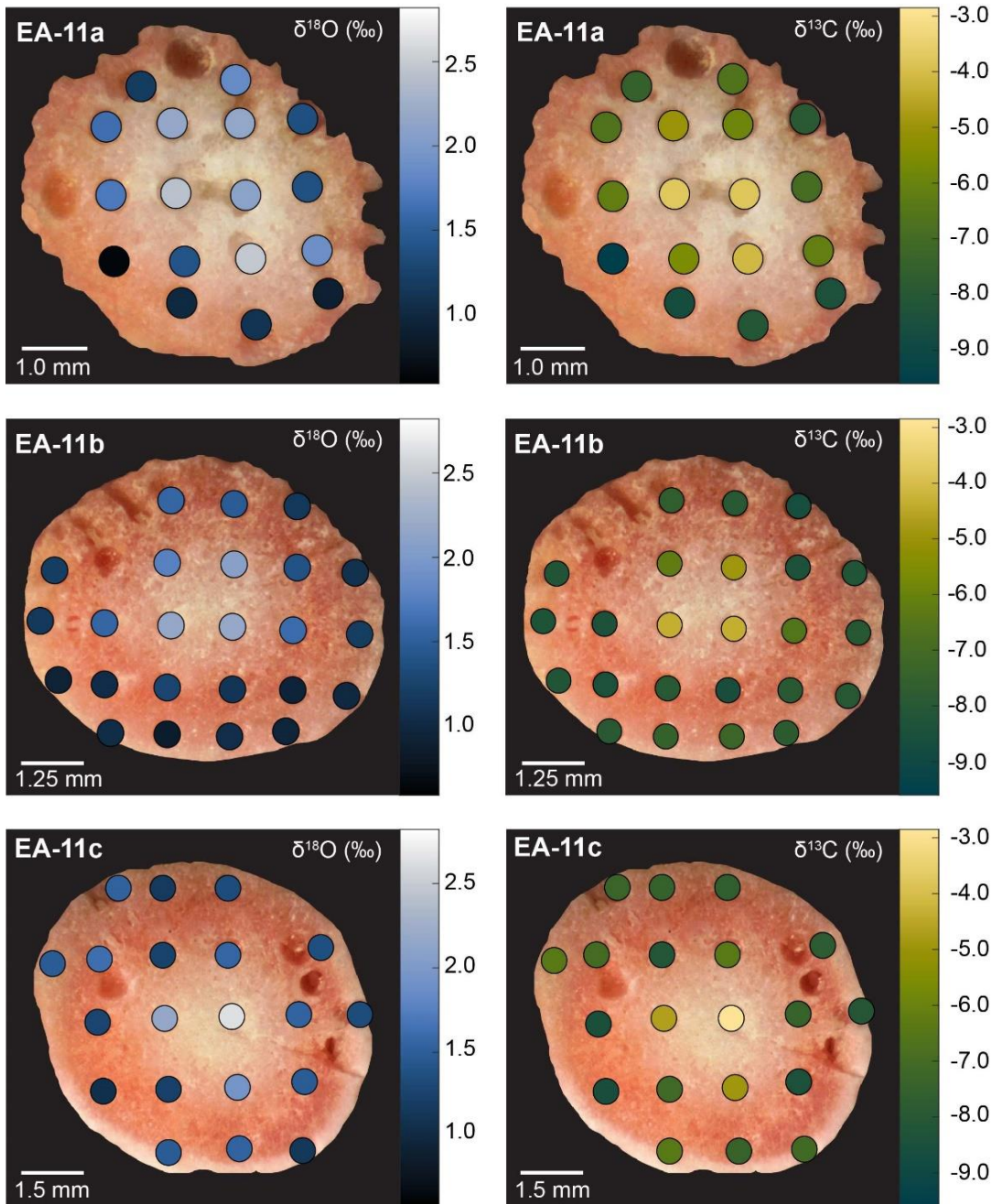
170 The interior coral skeletons lacked any visible banded growth structure that we expected to see in the manner of Samperiz et al. (2020) and Wisshak et al. (2009). Instead, the corals were characterized by a central white section, surrounded by shades of pink in the mid to outer sections (Figs. 2 and 3). The replacement of a high-density growth banding structure with the observed color blocking presents obstacles to conventional analyses: there are no annual growth structures from which to estimate the amount of time over which these corals have been growing, and there are no banding targets for stable isotope ratio subsampling. Thus, researchers aiming to analyze this coral taxon must employ additional radiometric dating techniques (e.g., Cheng et al., 2000) that are beyond the scope of this work. Because there were no visible banding targets for subsampling stable isotopes, the grid spacing of our sampling scheme allowed for microdrilling of several representative samples of both pink and white areas across each coral slice (Fig. S1).

Coral Slice	$\delta^{18}\text{O}$ (‰, PDB)		$\delta^{13}\text{C}$ (‰, PDB)		n
	Maximum	Minimum	Maximum	Minimum	
EA-11a	2.48	0.65	-3.72	-9.56	17
EA-11b	2.18	0.87	-4.34	-8.61	24
EA-11c	2.64	1.08	-2.84	-8.54	20
EA-11d	2.87	0.66	-2.64	-8.68	37
EA-12a	2.81	0.60	-3.19	-8.18	17
EA-12b	2.53	0.82	-3.00	-8.02	25
All	2.87	0.60	-2.64	-9.56	140
Linear Regression (All data, $\delta^{18}\text{O}$ vs $\delta^{13}\text{C}$)	Slope	Intercept	R ²	p-value	n
	2.88 (± 0.14)	-10.94 (± 0.22)	0.76	< 0.001	140

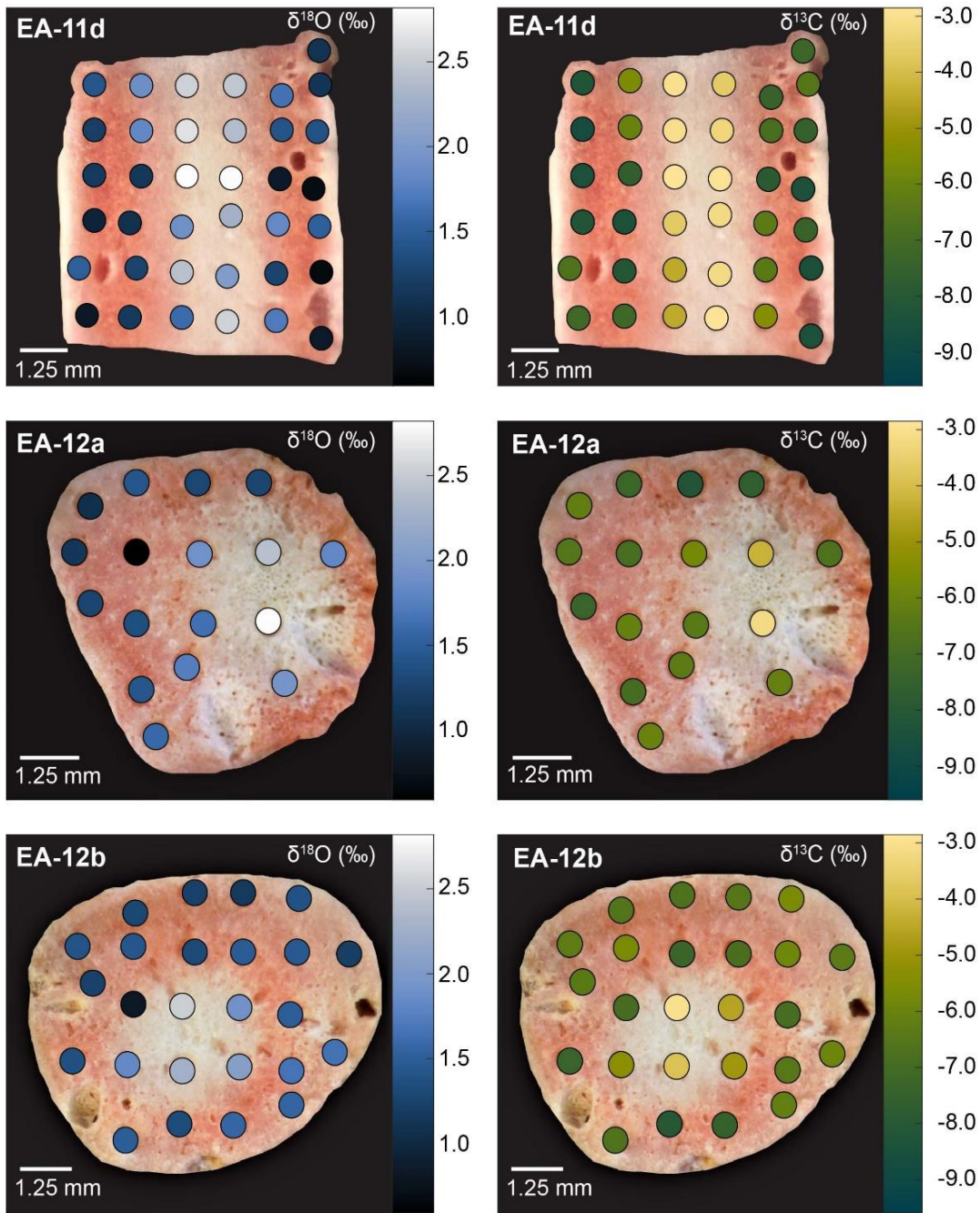
180 **Table 2:** Summary data for *E. fissurata* and regression statistics for the resulting compilation (see Fig. 5).

3.1 Stable carbon and oxygen isotope trends

Each coral slice exhibits a wide range of stable carbon and oxygen isotope ratios that are higher in the center, white section, and lower in the outer pink section of the coral (Fig. 3; Table S1). For specimen EA-11, the ranges in $\delta^{18}\text{O}$ and $\delta^{13}\text{C}$ values across slices EA-11a through EA-11c are ~ 1.5 ‰ and ~ 5.2 ‰, respectively. This variability is too large to produce accurate paleoceanographic records without knowledge of where the most accurate, or closest to that of an environmental signal, is preserved in the coral skeleton. The slightly larger range of $\delta^{18}\text{O}$ and $\delta^{13}\text{C}$ values observed over EA-11d (2.2 ‰ and 6.0 ‰, respectively) could be due to the sampling scheme for this slice covering a larger vertical distance of coral than the others (i.e., transecting more time intervals). The compilation of EA-11 $\delta^{18}\text{O}$ values ranges from 0.65 ‰ to 2.87 ‰, and the $\delta^{13}\text{C}$ values range from -9.56 ‰ to -2.64 ‰, with the minimum values exhibited by EA-11a (nearest the tip) and maximum values by EA-11d (far from the tip; Table 2). This trend is similar to that observed by Samperiz et al. (2020) for large, specimen-scale isotopic

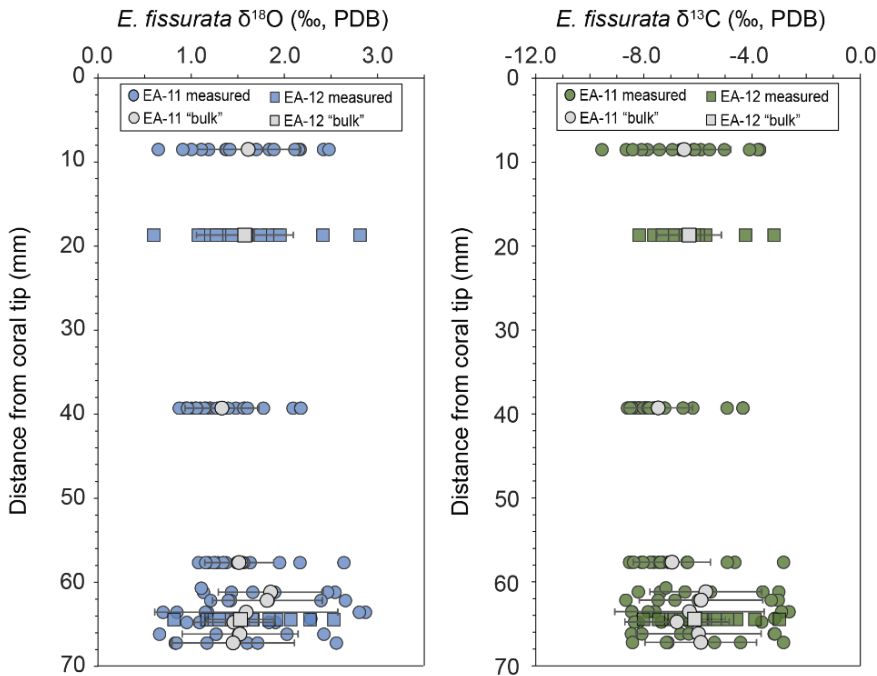


195 **Figure 3:** Stable isotope ratio maps for slices from specimens EA-11 and EA-12. Each horizontal pair of images show data from the same coral slice: the left column depicts $\delta^{18}\text{O}$ values and the right column $\delta^{13}\text{C}$ values. The measurements are presented as colored circles on each slice with corresponding adjacent color bar. Values are expressed in per mil (‰) relative to PDB, and analytical uncertainty (1σ) during this study was ± 0.064 ‰ $\delta^{18}\text{O}$ and ± 0.083 ‰ $\delta^{13}\text{C}$. All slices exhibit the same feature of the highest isotopic values toward the inner white section, which is not always the geometric center of the slice.



200 **Figure 3 continued.**

trends. The overall range of values, however, does not significantly change up-coral (Fig. 4).



205 **Figure 4:** Stable isotope ratios from each slice versus distance from the coral tips. On the left is $\delta^{18}\text{O}$ and on the right is $\delta^{13}\text{C}$; the analytical uncertainty for each is smaller than the data points. A “bulk” value was calculated as the average for each slice that would be similar to bulk drilling methods (except for EA-11d which was cut transverse to the growth axis and spans a range of distances, each averaged separately). Error bars on “bulk” calculations represent standard deviation for each slice (or distance from the tip). The “bulk” values do not vary along the growth axis.

210 For specimen EA-12, the range of $\delta^{18}\text{O}$ and $\delta^{13}\text{C}$ values over each of the slices is on the order of $\sim 2\%$ and $\sim 5\%$, similar to EA-11 (Table 2). The entire range of measured EA-12 $\delta^{18}\text{O}$ values is 0.60‰ to 2.81‰, and $\delta^{13}\text{C}$ values range from -8.18‰ to -3.00‰. Minimum $\delta^{18}\text{O}$ and $\delta^{13}\text{C}$ values for EA-12 were both exhibited by slice EA-12a, nearest the tip. The maximum values, however, were not on the same slice (maximum $\delta^{18}\text{O}$ at EA-12a and maximum $\delta^{13}\text{C}$ at EA-12b). Similar to EA-11, EA-12 also exhibits variability within each slice; however, this also leads to the “bulk” calculations not being significantly
 215 different from each other along the growth axis (Fig. 4). Looking closer at the individual slices from each coral, the variable stable isotope compositions are significant, i.e., the minimum and maximum values measured on each slice are well beyond the analytical uncertainty (Figs. 4 and 5). This supports that all measurements consistently demonstrate significantly higher $\delta^{18}\text{O}$ and $\delta^{13}\text{C}$ values in the center of each slice (Figs. 3 and 5).

3.2 Deviations from equilibrium with seawater $\delta^{18}\text{O}$ and $\delta^{13}\text{C}$

220 To determine where the *E. fissurata* skeletons record isotopic compositions most representative of an environmental signal, we calculated carbonate isotopic equilibrium values using data reported for nearby hydrographic stations. The seawater stable isotope ratios and temperature were determined using the average composition of the 490–650 m depth range (similar to the

coral collection depths; Table S2) at stations nearest the coral dredge sites (Fig. 1). For seawater $\delta^{18}\text{O}$, we gathered seawater temperature, potential temperature, and salinity records from CTD cast data from the AnSlope (Cross-slope exchanges at the Antarctic Slope Front) project that sampled very close to our dredge sites (Fig. 1 and Fig. S2) (Jacobs, 2015; Visbeck, 2015; Gordon, 2016). The average potential temperature ($-0.12 \pm 0.09^\circ\text{C}$) and salinity (34.7 ± 0.002) were used to identify the water mass at our locale and depth as Low Salinity Bottom Water, as described by Jacobs et al. (1985; Table S2). The reported $\delta^{18}\text{O}$ for this water mass is $-0.26 \pm 0.06\text{‰}$ (Jacobs et al., 1985). Determining seawater dissolved inorganic carbon (DIC) $\delta^{13}\text{C}$ was straightforward as direct measurements existed for nearby WOCE (World Ocean Circulation Experiment) stations (Fig. 1 and Fig. S2) (WOCE, 2002). Similar to the seawater $\delta^{18}\text{O}$, we calculated the average reported seawater DIC $\delta^{13}\text{C}$ values for our depth range for a value of $0.66 \pm 0.05\text{‰}$ (Table S2 and Fig. S2).

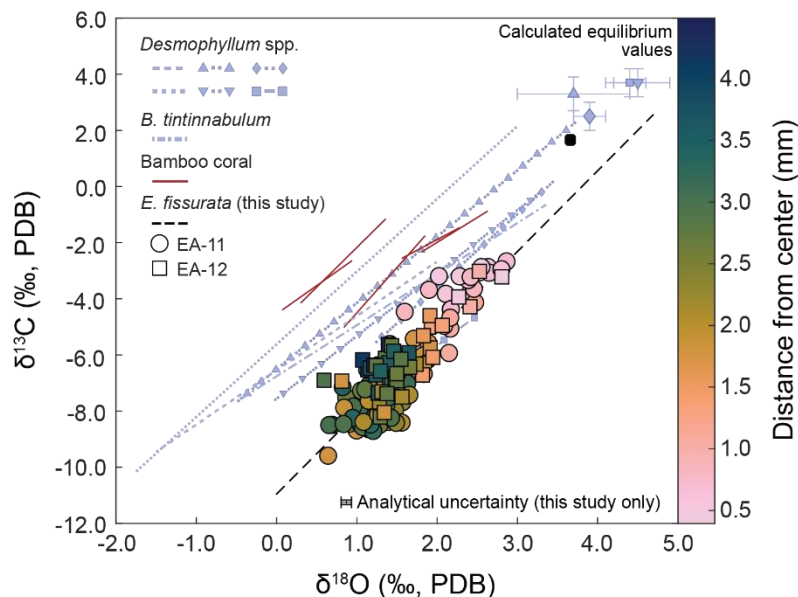


Figure 5: Linear regressions of $\delta^{18}\text{O}$ vs $\delta^{13}\text{C}$ values for *E. fissurata* compared to aragonitic scleractinian and calcitic bamboo corals. Colors of circles (EA-11) and squares (EA-12) correspond to distance from the coral center, see color bar at the right. Calculated seawater equilibrium value for *E. fissurata* is also shown as a black rounded square (uncertainty is smaller than the square). The dashed black line represents the line of best fit for the isotopic values measured here ($\delta^{13}\text{C} = 2.88 (\pm 0.14) * \delta^{18}\text{O} - 10.94 (\pm 0.22)$; $p < 0.001$). Linear regressions for *Desmophyllum* spp. are reported by Adkins et al. (2003) and include *Desmophyllum* sp. (purple line with squares) and *D. dianthus* (all other *Desmophyllum* lines). The dashed lines with shapes have corresponding equilibria displayed (matching shape with error bars in upper right corner). The *Bathypsammia tintinnabulum* was reported by Emiliani et al. (1978) and Bamboo coral data are from Hill et al. (2011). Lines for external data are not extrapolated beyond the range of reported $\delta^{18}\text{O}$ values. The slope of the linear regression produced in this study is similar to those reported for other deep-sea corals, with a similar magnitude decrease in both isotopic ratios from equilibrium. The measured values here that are closest to equilibrium are those toward the center of each coral disc.

The results from XRD analyses support the dominant presence of calcite with small amounts of aragonite in these specimens. The powdered samples of EA-11b yielded results of essentially identical compositions for both inner white and outer pink

sections with mostly calcite and <5% aragonite (Fig. S3). The color stripes that were analyzed from EA-11d also show only small differences between the white and pink compositions over a wider range of 2 θ (Fig. S3). Therefore, we calculated seawater equilibrium values relative to calcite using equations from O'Neil et al. (1969) and Romanek et al. (1992) for $\delta^{18}\text{O}$ and $\delta^{13}\text{C}$, respectively, which also allowed for comparison to published works. The resulting equilibrium $\delta^{18}\text{O}$ value was calculated to be 3.66 ± 0.06 ‰ and the equilibrium $\delta^{13}\text{C}$ value was 1.66 ± 0.20 ‰ (Fig. 5; Table S2).

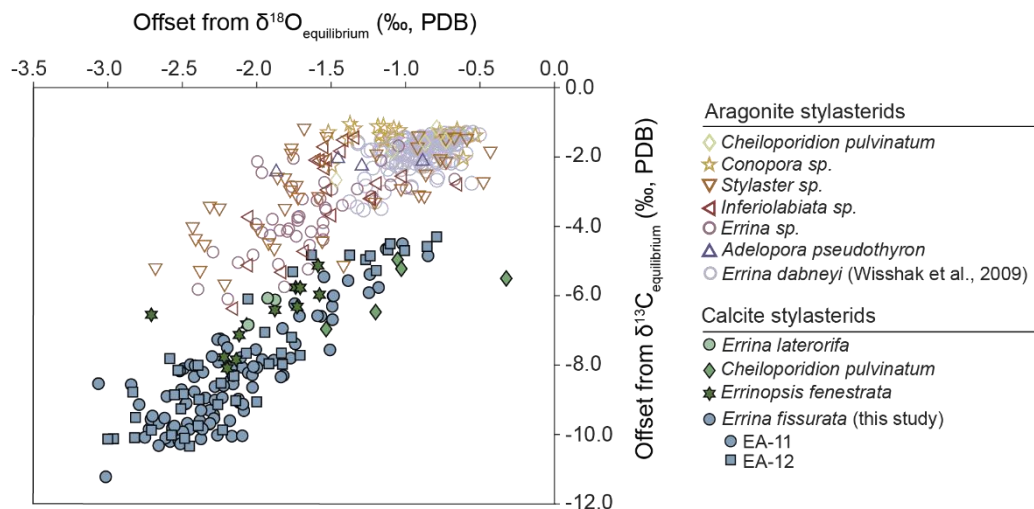


Figure 6: Difference between measured coral isotope ratios and equilibrium values for compilation of stylasterid corals. Except for *E. dabneyi* and *E. fissurata*, all coral isotope data are from Samperiz et al. (2020) and the corresponding equilibrium values were calculated using corresponding seawater data from Samperiz et al. and equations from Grossman and Ku (1986; aragonite $\delta^{18}\text{O}$ equilibrium), O'Neil et al. (1969; calcite $\delta^{18}\text{O}$ equilibrium), and Romanek et al. (1992; aragonite and calcite $\delta^{13}\text{C}$ equilibrium). *E. dabneyi* data and $\delta^{18}\text{O}$ equilibrium are from Wisshak et al. (2009), and the $\delta^{13}\text{C}$ equilibrium was calculated using reported seawater data from Wisshak et al. (2010). The corals from this study (blue filled circles and squares) exhibit a similar offset from equilibrium to other calcitic specimens (filled symbols). Some of the values closer to equilibrium (relative to calcite) from the *E. fissurata*, even overlap with aragonitic samples as well.

The values measured nearest to the center of each coral slice are consistently closest to calculated equilibrium, whereas the values from the mid to outer sections are further from equilibrium (Figs. 5 and 7). These equilibrium offsets are all negative in direction (i.e., the corals record isotopic ratios less than expected equilibrium) and range from -3.06 to -0.79 ‰ for $\delta^{18}\text{O}$ and from -11.22 to -4.30 ‰ for $\delta^{13}\text{C}$ (Fig. 6). The offsets from $\delta^{13}\text{C}$ equilibrium are considerably larger than $\delta^{18}\text{O}$ (Fig. 6). Additionally, we observe a strong linear correlation between $\delta^{18}\text{O}$ and $\delta^{13}\text{C}$ values. The compilation of samples in this study result in a linear trend with a slope of 2.88 ± 0.14 ($\Delta\delta^{13}\text{C}/\Delta\delta^{18}\text{O}$; $R^2=0.76$; $p<0.001$) or 0.26 ± 0.01 ($\Delta\delta^{18}\text{O}/\Delta\delta^{13}\text{C}$; $R^2=0.76$; $p<0.001$) that passes near the calculated equilibrium value (Fig. 5 and Table 2).

4 Discussion

4.1 Evaluation of major $\delta^{18}\text{O}$ and $\delta^{13}\text{C}$ trends

Stable oxygen and carbon isotope analysis of *E. fissurata* supports an influence of vital effects on the skeletal geochemistry of this stylasterid species. Because little is known about the biocalcification mechanisms and processes of stylasterid corals, we discuss here any similarities to other coral records and present new insights. Fractionation towards lower isotopic ratios relative to equilibrium as well as a positive correlation between $\delta^{18}\text{O}$ and $\delta^{13}\text{C}$ values has been well documented among skeletal records generated from different classes of corals (e.g., Emiliani et al., 1978; Swart, 1983; McConnaughey, 1989a; Smith et al., 2000; Adkins et al., 2003; Hill et al., 2011; Samperiz et al., 2020; Stewart et al., 2020). In Figure 5, we compare new data from this study with several scleractinian and bamboo corals. The linear regression between *E. fissurata* $\delta^{18}\text{O}$ and $\delta^{13}\text{C}$ values exhibits very similar slopes to other deep-sea corals and fall within similar ranges of isotopic compositions. This supports that vital effects can have a similar influence on corals of different classes (Weber and Woodhead, 1970), and across different latitudinal and depth ranges. Unlike the scleractinian corals analyzed by Adkins et al. (2003), *E. fissurata* does not exhibit a “break” in the slope of the linear regression (Fig. 4). This is supported by the findings of Stewart et al. (2022) wherein boron isotopes revealed that stylasterids do not upregulate the pH of their internal calcifying fluids to enhance calcification, thus altering the linear relationship between isotope ratios. An unusual isotopic trend from the *E. fissurata* corals is the innermost values of each sample disc approaching equilibrium (Figs. 3, 5, and 7). This contrasts the findings of Samperiz et al. (2020) who measured the innermost portion of *E. antarctica* as furthest from isotopic equilibrium (Fig. 7; note that the equilibrium value in this figure is for this study only, however, the *E. antarctica* isotope ratios clearly decrease towards the coral center). Additionally, Hill et al. (2011) sampled bamboo corals across a transect which resulted in $\delta^{18}\text{O}$ and $\delta^{13}\text{C}$ values further from equilibrium in the center of the coral (Fig. 7). Results from Wisshak et al. (2009) can only partially support these works as they generated $\delta^{13}\text{C}$ values from the center *E. dabneyi* that produced a single value from the innermost portion that was much lower than equilibrium (Fig. 7). Stable isotope ratios closer to equilibrium in the center of *E. fissurata* are the first of their kind for stylasterids and we posit that they imply lessening vital effects in this region because of slower calcification rates (McConnaughey, 1989b). Figure 7 also illustrates the wide range in isotopic variability exhibited by *E. fissurata* compared to the aragonitic *E. dabneyi*, *E. antarctica*, and calcitic bamboo corals (Wisshak et al., 2009; Samperiz et al., 2020; Hill et al., 2011, respectively). The range in isotope values that trend toward equilibrium in the center of the coral could be a result of a unique calcification strategy that also leads to a lack of visible banded structure within *E. fissurata*.

Rapid calcification rates, and therefore prominent vital effects have been interpreted as the reason that *E. antarctica* growth tips exhibit some of the lowest $\delta^{18}\text{O}$ and $\delta^{13}\text{C}$ values when compared to main trunk and branch samples (Samperiz et al., 2020).

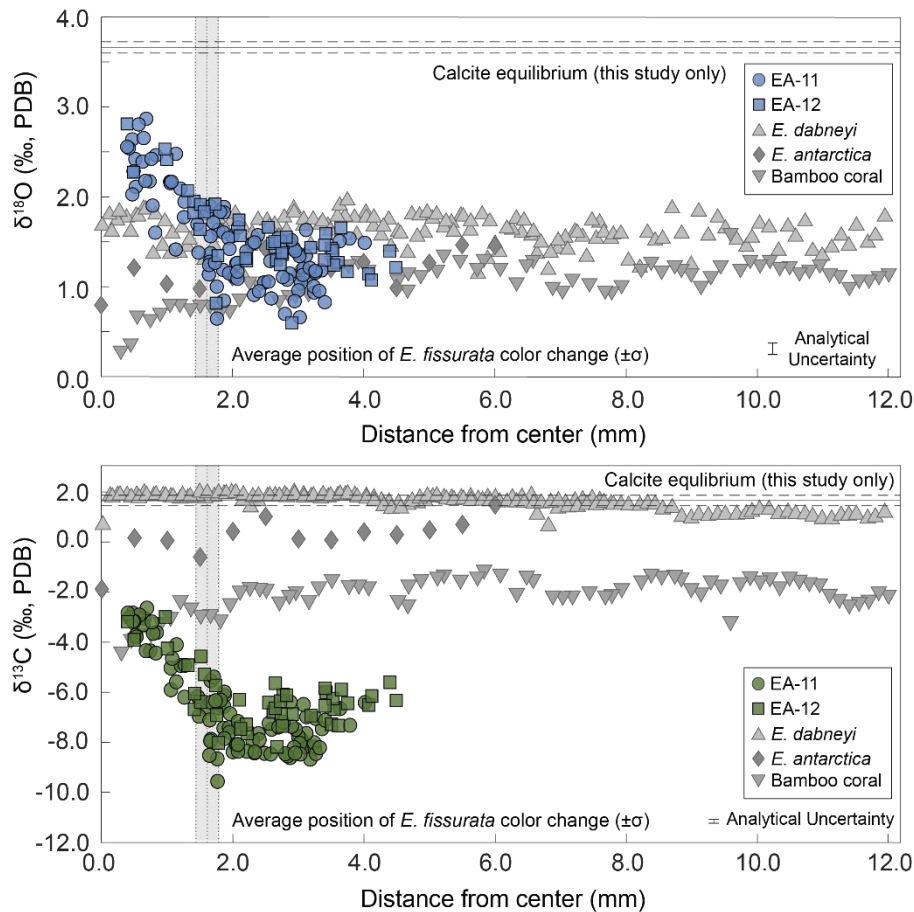


Figure 7: Oxygen (top) and carbon (bottom) stable isotope ratios by distance from the center of the coral. The values from this study are plotted by slice from each specimen as noted by the colored circles (EA-11) and squares (EA-12). The horizontal lines denote calculated calcite equilibrium values for this study with corresponding uncertainty in dashed lines ($\pm 1\sigma$). Vertical gray bars denote the average radius of the white coral center for *E. fissurata*, the width of the bar denoting $\pm 1\sigma$. Also included are additional coral data sampled in a similar transect style. *E. dabneyi* is from Wisshak et al. (2009), *E. antarctica* is from Samperiz et al. (2020), and the bamboo coral data are from Hill et al. (2011). Regarding $\delta^{18}\text{O}$, the *E. antarctica* and bamboo coral seem to have a small decrease in the last few datapoints toward the center. Regarding $\delta^{13}\text{C}$, the same is true of each of the corals from other studies. This contrasts the increase we observe within our corals.

Here, the most negative $\delta^{18}\text{O}$ and $\delta^{13}\text{C}$ values for EA-11 were measured on the slice closest to the tip, EA-11a, and the most positive $\delta^{18}\text{O}$ and $\delta^{13}\text{C}$ values were measured on a slice furthest from the tip, EA-11d (Table 2). Specimen EA-12 was characterized by $\delta^{18}\text{O}$ and $\delta^{13}\text{C}$ minima nearest the tip (EA-12a), but the maximum isotope ratios were measured on different slices: the most positive $\delta^{18}\text{O}$ was closer to the tip and the most positive $\delta^{13}\text{C}$ was further away (Fig. 4 and Table 2). These observations, however, are not a direct comparison to measurements by Samperiz et al. (2020) for two reasons. First, the sampling scheme here was designed to exploit isotopic variability across a coral slice, thus considering calculated “bulk” values from each slice should provide more comparable value. However, our calculated “bulk” values do not exhibit any

significant changes over the lengths of the corals; they all exhibit similar variance along their respective coral and are within error of each other (Fig. 4). This could be due to the second limitation on comparisons: we did not sample the true tips of the corals, but instead were ~1 cm below, possibly preventing us from sampling the most negative $\delta^{18}\text{O}$ and $\delta^{13}\text{C}$, so we cannot truly compare growth tips. We are also uncertain of the lower extent of EA-11 and EA-12, as they were dredge collected, and could be missing a portion of the main trunk, possibly preventing us from sampling the most positive $\delta^{18}\text{O}$ and $\delta^{13}\text{C}$ (Fig. 2).

An additional influence on skeletal $\delta^{18}\text{O}$ and $\delta^{13}\text{C}$ values of stylasterid corals is carbonate mineralogy. It has been widely known that fractionation of stable oxygen and carbon isotopes occurs between carbonate and seawater, the magnitude of which is different for aragonite and calcite (e.g., O'Neil et al., 1969; Grossman and Ku, 1986; Swart, 1983; Romanek et al., 1992). This has been observed in abiotic laboratory precipitation experiments, as well as organisms that precipitate carbonate shells or skeletons (Romanek et al., 1992; Lécuyer et al., 2012; Samperiz et al., 2020, respectively). In addition to taxonomical organization, mineralogical content has recently become a common method by which to categorize specimens when analyzing skeletal geochemistry (Stewart et al., 2020; Samperiz et al., 2020; Stewart et al., 2022; Kershaw et al., 2023). The *E. fissurata* here are mainly calcite with <5% aragonite (Fig. S3). The bulk sample scanned from EA-11d would be most comparable to the bulk mineralogy data reported in the literature, but the subsamples of coral color bands are the first of their kind. The peak intensities from the scanned coral color bands show some minor differences between the pink and white, however, the analysis of pulverized samples from EA-11b demonstrate nearly identical mineral content (Fig. S3). This work presents the first stylasterid mineralogical data obtained by methods other than bulk sample analysis. The *E. fissurata* $\delta^{18}\text{O}$ and $\delta^{13}\text{C}$ values align well in isotope space with other calcitic stylasterids; they are further offset from isotope equilibrium than their aragonitic counterparts along the $\delta^{13}\text{C}$ axis, but within range of the aragonitic $\delta^{18}\text{O}$ values (Fig. 6).

4.2 Surveying maps of skeletal stable isotope composition: alternative mechanisms for high central $\delta^{18}\text{O}$ and $\delta^{13}\text{C}$ values

4.2.1 Organic contribution to outer skeletal portion

Stylasterid corals have been observed hosting other species including boring cyanobacteria, sponges, and gastropods, all of which could affect the isotopic composition of the coral skeleton (Puce et al., 2009; Braga-Henriques et al., 2010; Pica et al., 2015). The presence of such organisms could contribute metabolic carbon and/or oxygen to the pool from which the corals calcify, similar to the metabolic effects of shallow-water coral symbionts (e.g., McConnaughey, 1989a). Depending on the relationship of the epiphyte, and if it is living near an active calcification site, isotopically light metabolic products could be incorporated into the coral carbonate, driving the outer portions of the coral to lower $\delta^{18}\text{O}$ and $\delta^{13}\text{C}$. There have been direct observations of barnacles living on *E. fissurata* (Pica et al., 2015). For specimen EA-11, sections with any obvious external growth or signs of hosting were avoided and only clean slices were selected for sampling. For EA-12, however, this coral was believed to be dead upon collection, and covered in possible organic growth/encrustation over time (Fig. 2). We posit that this material was not present at the time of coral calcification and therefore would not have altered the $\delta^{18}\text{O}$ and $\delta^{13}\text{C}$ values of the carbonate. The similarity in isotope trends between both specimens supports this hypothesis.

345 4.2.2 Diagenetic influence on stable isotopic composition

Coral diagenesis can be described as a post-calcification alteration of carbonate geochemistry. Such alteration processes could directly change the skeletal $\delta^{18}\text{O}$ and $\delta^{13}\text{C}$ values by removing or replacing the carbonate. Identifiable diagenetic features for stylasterid corals have been described by Black and Andrus (2009), including encrustation of foreign materials on the outer surface of the coral skeleton, microspar fabric and microbioclastic debris, abrasions, fragmentation, pitting, and bioerosion. 350 Black and Andrus (2009) identified these features on fossil and modern corals using scanning electron microscopy (SEM) but found no impact on the $\delta^{18}\text{O}$ and $\delta^{13}\text{C}$ of their specimens. Work by Wisshak et al. (2009) has identified additional diagenetic impacts on stylasterid corals via micro-scale dissolution and re-precipitation. We were able to analyze *E. fissurata* live-collected specimens EA-22, EA-23, and EA-24 for physical signs of diagenesis (Figs. S4 and S5 for example of EA-24). Although we did not image specimens EA-11 or EA-12, the others were collected from the same dredges. We imaged slices 355 of coral branches similar to the stable isotope sampling scheme and did not see any signs of the diagenetic effects described, except for possible secondary growth or recrystallization (Figs. S4 and S5). Although we have identified evidence of secondary crystal growth, the scale is on the order of $\sim 100\ \mu\text{m}$. That size is 5 times smaller than the size of the drill bit used here, and therefore unlikely to have an impact on the $\delta^{18}\text{O}$ and $\delta^{13}\text{C}$ variability observed.

4.2.3 Calcite versus aragonite mineralogy

360 With the XRD data presented here, there is evidence for a predominantly calcite skeleton for *E. fissurata*. This is important to consider in terms of both growth models and temperature reconstructions. Comparing $\delta^{18}\text{O}$ and $\delta^{13}\text{C}$ values from eight specimens of *Cheiloporidion pulvinatum* (five purely aragonite and three purely calcite) collected from the same location resulted in an average difference of $\sim +1.4\ \text{‰}$ $\delta^{18}\text{O}$ and $\sim +5.3\ \text{‰}$ $\delta^{13}\text{C}$, the higher values being aragonite (Samperiz et al., 2020). Based on the results here, we have evidence for a negligible effect of mineralogy as a potential driver for the change in 365 isotope composition toward the center of these corals (Fig. S3). However, with apparent mineralogical variability among the Errina genus (see Fig. 6; Cairns and Macintyre, 1992), it would be prudent to assume some variability among individuals within a species, and thus mineralogy must be considered as an important variable in *E. fissurata* biocalcification and use as a paleoceanographic archive.

4.3 Hypothesized large-scale calcification model for *E. fissurata*

370 To further investigate the possibility of vital effects leading to specimen-scale differences in $\delta^{18}\text{O}$ and $\delta^{13}\text{C}$ values, we posit that *E. fissurata* calcifies in a way that magnifies the vital effects in the outer region compared to the center. In order to grow dendritically, the most intuitive growth model for corals such as our stylasterids holds that the center of each branch extends axially faster than each branch thickens radially. Thus, the kinetic effects would be most apparent in the center of each coral slice and lessen towards the outer edges, resulting in $\delta^{18}\text{O}$ and $\delta^{13}\text{C}$ values that would therefore approach equilibrium toward 375 the edges of each isotope map. Many marine calcifying organisms (e.g., mollusks and corals) follow the Von Bertalanffy

growth model wherein their calcification rate ontogenetically decreases, and we posited that this model also applied to the horizontal extension of stylasterids as they prioritize vertical growth (Ralph and Maxwell, 1977; Emiliani et al., 1978; Berkman, 1990; Philipp et al., 2005; Román-González et al., 2017). Such a coral growth model is supported by observations from Fallon et al. (2014) wherein a cold water scleractinian coral demonstrated growth similar to stacking cones with a fast growing tip. This structure is also supported by isotopic records of other stylasterids and bamboo corals which were all characterized by low isotopic values at the regions of most rapid growth (Wisshak et al., 2009; Samperiz et al., 2020; Hill et al., 2011).

To better understand our resulting trends, we created models that reflect simplified calcification scenarios of constant, decreasing, and increasing radial extension with time. The model calculations were based on an idealized coral slice of n rings with radii, r_{n+1} , an initial growth inner circle of radius, r_1 , and the extension rate represented by the change in radius, Δr , between each ring (Fig. 8). We set each model to run for 100 years and examined the rate of change of coral area as a proxy for calcification rate in each scenario. Whereas few studies have determined vertical growth rates of deep-sea stylasterid corals (Stratford et al., 2001; Chong and Stratford, 2002; Miller et al., 2004; Wisshak et al., 2009; King et al., 2018), their radial extension rates remain largely unknown. Therefore, we employed a range of radial growth rates reported for live-collected bamboo corals living at a depth of 1000–1700 m (Thresher et al., 2011). The bamboo corals were reported to grow from 0.01–0.12 mm y^{-1} ; therefore, our constant radial extension scenario was characterized by the median 0.065 mm y^{-1} (Fig. 9a–c). The decreasing radial extension scenario was initially set to the maximum extension rate of 0.12 mm y^{-1} that decreased linearly by 0.0011 mm y^{-2} until the minimum growth rate of 0.01 mm y^{-1} was reached at 100 years (Fig. 9d–f). For the increasing radial extension scenario, the opposite was set, an initial radial extension rate of the minimum 0.01 mm y^{-1} and a linear increase at a rate of 0.0011 mm y^{-2} until 0.12 mm y^{-1} at 100 years (Fig. 9g–i).

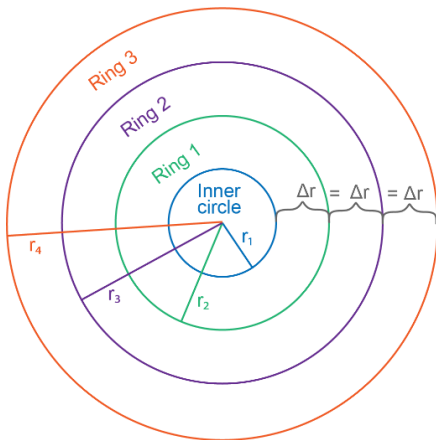
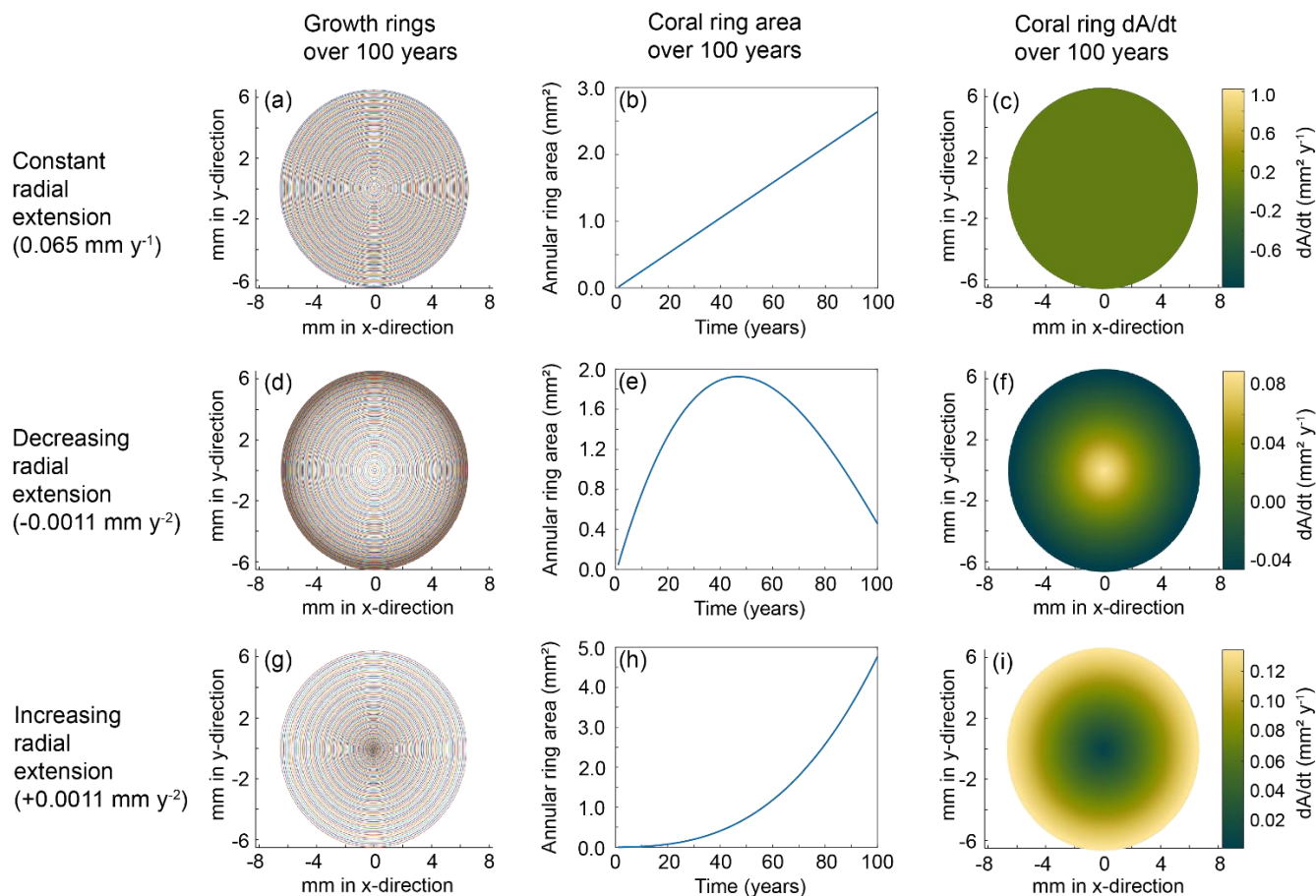


Figure 8: Coral slice schematic used for calcification models. In this simplified model, growth begins with the inner circle of radius r_1 . Each growth increment is noted by a new ring, Ring n , with a radius, r_{n+1} . In this case, the change in radius between

each ring, Δr , is equal representing the constant radial extension model. The Δr becomes larger or smaller with each ring for
400 the increasing and decreasing growth scenarios, respectively.

We observe stronger vital effects toward the outer edges of the *E. fissurata* coral slices and interpret this as increased calcification rate along the outer edges. To test if this growth scenario likely represents our stable isotope maps, we defined changes in calcification rate as the two-dimensional changes in coral area with time. We then compared the resulting models to the changes in stable isotope values across each coral slice (assuming no change in the ambient seawater values during the
405 time of precipitation). In the case of the constant radial extension, the growth rings are evenly spaced, leading to a steady increase of horizontal area between the rings with time (Fig. 9a and b). Constant radial extension refers to constant change in area with time (Fig. 9c). Such a growth model would result in stable isotope values to either be constant across the surface of the coral or record any changes that reflect seawater variability. Decreasing radial extension with time relates to decreasing area with time (Fig. 9d–f) and would be the most likely calcification pattern as the available literature supports slowing growth
410 with time among marine carbonates (Ralph and Maxwell, 1977; Emiliani et al., 1978; Berkman, 1990; Philipp et al., 2005; Román-González et al., 2017). With decreasing radial extension, the growth bands become closer with time, causing the area to increase then decrease over the modeled 100-year span (Fig. 9d and e). Therefore, the rate of change of area decreases toward the outer edges of the coral surface (Fig. 9f) and the center of the coral would exhibit isotope values furthest from equilibrium. That is the opposite of what we observed with *E. fissurata*. The increasing radial extension scenario led to growth
415 bands increasing distance from each other, resulting in an exponential increase in area (Fig. 9g and h). The resulting calcification scheme (i.e., rate of change in area) would lead to stronger vital effects toward the outer edges of the coral surface and isotopic values closer to equilibrium in the center (Fig. 9i) as observed with *E. fissurata*.



420 **Figure 9:** Coral calcification models for each scenario. The top row (a–c) depicts results from the constant radial extension model, the middle row (d–f) is the decreasing radial extension, and the bottom row (g–i) is the increasing radial extension model. The left column depicts the growth rings for each model after a run of 100 years. The middle column shows the change in area with each year of calcification. The right column shows the rate of change in coral area for each model. The corresponding color bars represent the magnitude of change.

425 If driven by calcification scheme, the unique pattern presented here of the highest isotopic values in the center of the coral with lower values toward the mid and outer edge supports a model of rapid calcification toward the outer region and slower calcification in the center. Such a model, however, is not supported by previously mentioned growth habits of marine carbonates and would not be expected to result in dendritic corals. To reconcile these contradictions, we explore calcification strategies that invoke uneven, or two-step biomineralization to account for the spatial distribution of vital effects observed in our coral isotope maps.

430 A growth model of shallow water staghorn coral (*Acropora cervicornis*) over daily to yearly timescales reconciles our data (Gladfelter 1982, 1983, 1984). The Gladfelter model includes two main phases: rapid extension by randomly oriented crystals that develop the main skeletal framework, followed by infilling and strengthening of the skeleton along the entire growth axis (Gladfelter, 1982). Gladfelter (1983) observed that the initial framework growth was largely around the mid and outer regions

of the corallite and the infilling occurred later in the center. We posit that the basic premise of this model (rapid initial growth followed by slower calcification) describes the coral growth presented here. The lower isotopic values toward the outer edge
435 signify enhanced kinetic fractionation from the rapid growth. The center region of the coral calcifies at a slower rate; thus, kinetic fractionation is reduced resulting in higher isotopic values closer to equilibrium. We acknowledge that the Gladfelter growth model employs fusiform crystals setting a foundation upon which bundles of aragonite crystals grow, and we are not able to determine that scale of calcification here. We instead posit that because of our consistent spatial isotopic discrepancies, and our contrast to previous stylasterid works, there must be a heterogeneous growth structure for *E. fissurata* not previously
440 described for stylasterids, and the growth described by Gladfelter (1983) does this.

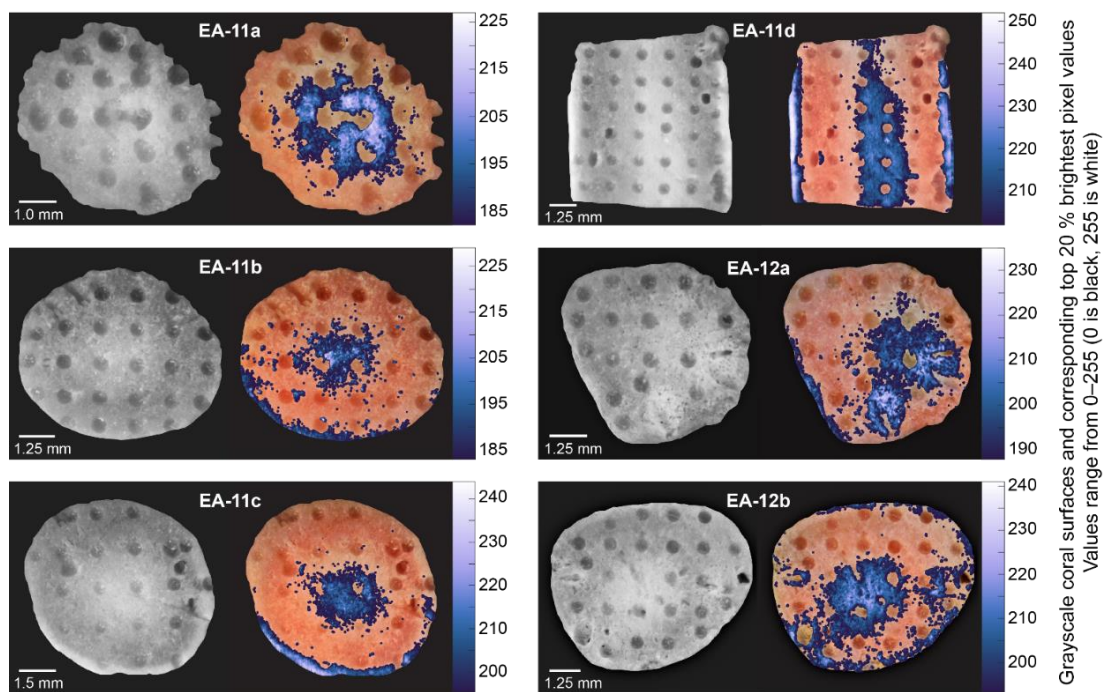
A final consideration for growth mechanisms driving the $\delta^{18}\text{O}$ and $\delta^{13}\text{C}$ trends in *E. fissurata* is that of the internal structures described for stylasterids. The stylasterid *Inferiolabiata labiata* was originally described by Moseley (1878, previously *Errina* (*Errina*) *labiata*). Internal decalcified structures of *Errina* were described in this work including the coenosarcal mesh, which is a network of small canals just below the coral surface that increased in size and distance from each other deeper into the
445 coral (Moseley, 1878). Wisshak et al. (2009) also observed these structures in their analysis of *E. dabneyi* microstructures. Vacuum-resin-embedded and decalcified coral branches were observed to have very dense meshwork of canals near the outer surface of the corals which became wider, deeper inside (Wisshak et al., 2009). Puce et al. (2012) employed volume rendering methods using X-ray computed microtomography to identify microstructures of *Distichopora* specimens. This work agreed with the canal networks that are small near the surface of the coral and larger inside (Puce et al., 2012). Combined, these works
450 support an uneven calcification mechanism for these few stylasterids that could also apply to *E. fissurata*. The small, densely packed meshwork near the outer edges of the coral surface would have much more surface area than the larger, less dense canals in the coral interior. Therefore, the outer regions would require faster calcification rates to keep up growth of the entire coral colony. This uneven rate of calcification would impose vital effects in the outer regions of *E. fissurata* if a similar growth pattern were occurring, leaving the center region closest to isotopic equilibrium.

455 **4.4 Considerations for paleoceanographic reconstructions**

Increasing isotopic values toward the inner, white section of the coral with minimal concurrent mineralogical change supports sampling *E. fissurata* branch and stem centers for paleotemperature reconstructions. This recommendation and subsequent discussion for this section are based on the nature of the coral mineralogy determined for these specimens; however, coral mineralogy should be assessed as part of future work as it will affect geochemical interpretations. Because the higher values
460 are located nearest the white section of the coral and not the geometric center, we converted the images of each slice to grayscale (Fig. 10). This allowed us to find the whitest pixels and quantitatively determine the most ideal location for sampling. With the exception of the light outer edges, the sample holes that were at least 75 % surrounded by the whitest pixels were selected for temperature reconstructions (Fig. 10). These $\delta^{18}\text{O}$ values were averaged for each coral slice and, in the absence of a calcite $\delta^{18}\text{O}$ temperature calibration for stylasterids, we use the temperature calibration equation from Samperiz et al. (2020).

465 This equation was established for 100% aragonite stylasterid corals and it is unclear if this is appropriate for our predominantly calcite *E. fissurata*. Additionally, the $\delta^{18}\text{O}$ average for each entire slice was calculated to determine a “bulk” value that would represent a sampling method of drilling across the growth axis (King et al., 2018; Samperiz et al., 2020). The calculated “bulk” $\delta^{18}\text{O}$ values were also calibrated to temperature and the results are illustrated in Fig. 10 (Table S3). Note that for slice EA-11d that consists of a vertical face rather than horizontal, $\delta^{18}\text{O}$ values were only combined for the same distance from the coral tip.

470



475 **Figure 10:** Compilation of grayscale images and corresponding brightest pixels (highest 20 %) over each coral slice. The colors correspond to the grayscale pixel value (higher on the scale bar denotes a whiter pixel). The sample holes surrounded by at least ~75 % of bright pixels were used to calculate representative $\delta^{18}\text{O}$ values for each slice for temperature calibration (Table S3).

Although both the “central” and calculated “bulk” temperature records are higher than current ocean temperatures of a similar depth, the center values are significantly different from calculated “bulk” measurements and are closer to the true environmental signal (Fig. 11). We compared the center and calculated “bulk” temperature records using the Student’s t-Test to determine whether the difference between the means is significant or occurred by chance (from variability). We used a paired t-Test to compare center and calculated “bulk” temperatures from the same distance from the tip where available. With a p-value of 6.61×10^{-6} , the difference between center and calculated “bulk” temperatures is very unlikely to have occurred by chance (Table S4). This analysis, however, assumes no environmental change over the lifespan of the corals. To account for possible seawater changes and to more accurately reflect the samples that would be targeted for temperature reconstructions,

480

we also tested individual temperatures across each slice (rather than the averages used in Fig. 11). The unpaired t-Test required
485 at least two temperature values that were sampled from the white center and the pink outer regions for at least one degree of
freedom. This was met by four coral slices, EA-11a, EA-11b, EA-11d (63.55 mm from the tip), and EA-12b; each test
producing p-values less than 0.005 (Table S4). These analyses show that we can conceive of no comparison within coral slices
that show the same values between the center and calculated “bulk” temperatures.

Figure 11 shows that detailed analysis of isotopic distributions through *E. fissurata* skeletons does not quite achieve samples
490 representative of isotope equilibrium; but a closer approach is possible. Computerized tomography (CT) scanning methods
could be employed in future research to identify possible density banding of skeletal structure not visible using standard
microscopy or SEM. Such visualization could enable even finer-scale samples than those achieved here. We posit that our
prescribed sampling scheme for these calcitic corals, paired with CT-guided sampling, may yield robust paleotemperature
records. Sampled as we have, with even distribution of samples over the surface of each disc as a goal, our reconstructed
495 temperatures are higher than a likely environmental signal (Fig. 11). However, we have demonstrated that the center white
region of these corals is less affected by vital effects and less likely altered after initial deposition. Therefore, because the coral
mineralogy is also minimally changed across each slice, we recommend sampling of the white center using more spatially
precise micro-milling methods to target even smaller regions, thus minimizing the impact of vital effects. We also note that in
calculating uncertainty associated with temperature calibrations, our center temperature errors are likely underestimated as
500 they rely largely on analytical uncertainty. However, our calculation of temperatures from calculated “bulk” data includes high
spatial standard deviations; more precise sampling would yield more precise temperature estimates. Thus, a targeted milling
approach would likely reflect a more accurate uncertainty estimate on the temperature as well. Additionally, CT scanning that
reveals coral growth structures, such as Puce et al. (2011), would allow an even closer approach to accurate paleoceanographic
reconstructions. Such combined methods would allow for extremely targeted sampling considering both the growth structure
505 and biomineralization methods to inform sampling efforts to allow closer approach to equilibrium and better accuracy of
paleotemperature reconstructions using *Errina* corals.

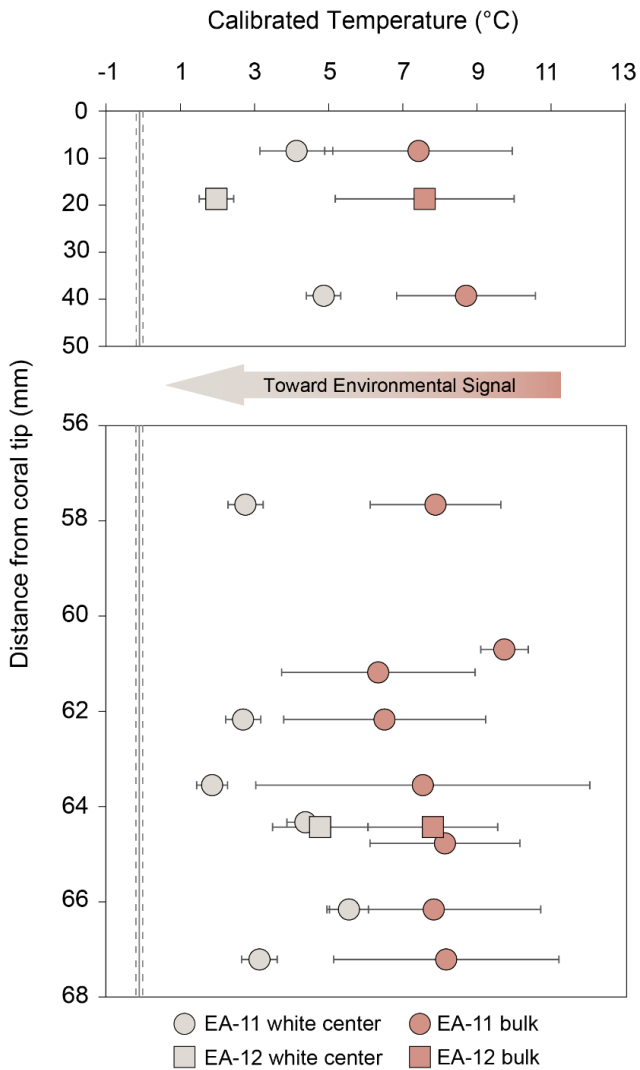


Figure 11: Comparison to temperature calibration using the equation from Samperiz et al. (2020) for aragonite stylasterid corals. Light colored points denote temperatures using the $\delta^{18}\text{O}$ values from the white centers of each slice, whereas the darker, peach color denote a “bulk” measurement. The “bulk” is calculated using the average $\delta^{18}\text{O}$ of the entire slice, similar to a value that would be measured from a sample collected via drilling into the side of a coral specimen. Error bars are based on standard deviation of three or more averaged samples. The error bars for less than three samples are based on the analytical error propagation (Table S3).

5 Conclusions

The results presented here contribute to a new understanding of the highly diverse family of stylasterid corals. In the case of *E. fissurata*, stable isotopic records provide geochemical details over a unique sampling resolution. We have demonstrated that *E. fissurata* skeletons exhibit significant and variable vital effects that obscure the environmental signal of this potential

paleoceanographic archive. Lacking any visible banding structure, the specimens in this study benefitted from a gridded sampling scheme to determine the location of minimum influence from vital effects. Our skeletal $\delta^{18}\text{O}$ and $\delta^{13}\text{C}$ values exhibit an increasing trend toward seawater equilibrium near the center of the coral. This result contradicts growth structures hypothesized in the current body of literature based on observed stable isotopic trends that have only focused on microsampling purely calcitic or purely aragonitic specimens (Wisshak et al., 2009; Samperiz et al., 2020; Hill et al., 2011). We posit that the observed trend in $\delta^{18}\text{O}$ and $\delta^{13}\text{C}$ values could be a result of heterogeneous growth/calcification structure. Possible growth strategies include (i) a two-stage growth model with a “hasty” initial lattice framework construction, followed by slower infilling to strengthen, and support the coral colony (Gladfelter, 1982, 1983) or (ii) rapid calcification around the outer edges of the coral stem to construct the dense canal meshwork that is more sparse towards the center (Moseley, 1878; Wisshak et al., 2009; Puce et al., 2012). We tested our interpretations that the $\delta^{18}\text{O}$ values from the center white region of the corals were closest to equilibrium by calibrating them to seawater temperature using the paleotemperature equation developed by Samperiz et al. (2020) for aragonite stylasterids. These $\delta^{18}\text{O}$ values produced temperatures significantly different than a “bulk” approach and were closest to nearby ocean temperatures. Thus, so long as coral mineralogy is spatially consistent, we recommend sampling this taxon along the center, white region where the carbonate geochemical record is closest to seawater equilibrium and an environmental isotopic signal. Further, we suggest initial CT scanning of corals to determine any hidden growth features, and micro milling sampling techniques to target the location of the most accurate record. Combined with continued efforts to develop stylasterid temperature calibrations, we posit that accurate paleotemperature records can be reconstructed from deep-sea *E. fissurata* corals.

Data availability

All data are available in the supplement and will be published on PANGAEA.

Author contributions

TMK and BER conceptualized the work. TMK developed sampling methods under the supervision of BER. NPJ provided expertise on mineralogical analyses. All authors contributed to formal analysis. TMK wrote the manuscript draft, with significant input from BER and NPJ. All authors approved the final version of the manuscript.

Competing interests

The authors declare that they have no conflict of interest.

Acknowledgements

545 We thank the captain, crew, and scientific staff of the RV *Nathaniel B. Palmer* during the US Antarctic Program expedition NBP07-01 to the Ross Sea, Antarctica for their efforts in coral collection. We also thank Dr. Ernst Peebles for the use of laboratory space during coral sampling, and Drs. Jennifer Granneman and David Jones for guidance on both slicing the corals and initial setup of the MircoMill. We also thank Dr. Lukasz Wojtas for providing XRD analysis at the University of South Florida and guidance during sample preparations. During this project, TMK was funded through the Genshaft Family
550 Dissertation Fellowship awarded by the University of South Florida as well as three endowed fellowships from the College of Marine Science: Carl Riggs Endowed Fellowship, George Lorton Fellowship in Marine Science, and the Abby Sallenger Memorial Award.

References

- 555 Adkins, J. F., Cheng, H., Boyle, E. A., Druffel, E. R. M., and Edwards, R. L.: Deep-Sea Coral Evidence for Rapid Change in Ventilation of the Deep North Atlantic 15,400 Years Ago, *Science*, 280, 725–728, <https://doi.org/10.1126/science.280.5364.725>, 1998.
- Adkins, J. F., Boyle, E. A., Curry, W. B., and Lutringer, A.: Stable isotopes in deep-sea corals and a new mechanism for “vital effects,” *Geochim. Cosmochim. Ac.*, 67, 1129–1143, [https://doi.org/10.1016/S0016-7037\(02\)01203-6](https://doi.org/10.1016/S0016-7037(02)01203-6), 2003.
- 560 Allemand, D. and Benazet-Tambutte, S.: Dynamics of calcification in the mediterranean red coral, *Corallium rubrum* (Linnaeus) (Cnidaria, Octocorallia), *J. Exp. Zool.*, 276, 270–278, [https://doi.org/10.1002/\(SICI\)1097-010X\(19961101\)276:4<270::AID-JEZ4>3.0.CO;2-L](https://doi.org/10.1002/(SICI)1097-010X(19961101)276:4<270::AID-JEZ4>3.0.CO;2-L), 1996.
- Andrews, A. H., Cordes, E. E., Mahoney, M. M., Munk, K., Coale, K. H., Cailliet, G. M., and Heifetz, J.: Age, growth and radiometric age validation of a deep-sea, habitat-forming gorgonian (*Primnoa resedaeformis*) from the Gulf of Alaska, *Hydrobiologia*, 471, 101–110, <https://doi.org/10.1023/A:1016501320206>, 2002.
- 565 Arndt, J. E., Schenke, H. W., Jakobsson, M., Nitsche, F. O., Buys, G., Goleby, B., Rebesco, M., Bohoyo, F., Hong, J., Black, J., Greku, R., Udintsev, G., Barrios, F., Reynoso-Peralta, W., Taisei, M., and Wigley, R.: The International Bathymetric Chart of the Southern Ocean (IBCSO) Version 1.0-A new bathymetric compilation covering circum-Antarctic waters: IBCSO VERSION 1.0, *Geophys. Res. Lett.*, 40, 3111–3117, <https://doi.org/10.1002/grl.50413>, 2013.
- 570 Berkman, P. A.: The population biology of the Atarctic scallop, *Adamussium colbecki* (Smith 1902) at New Harbor, Ross Sea, in: *Antarctic Ecosystems*, edited by: Kerry, K.R. and Hempel, G., Springer, Berlin, Heidelberg, Germany, 281–288, https://doi.org/10.1007/978-3-642-84074-6_32, 1990.
- Black, H., and Andrus, C. F. T.: Taphonomy and diagenesis on the deep-sea hydrocoral *Stylaster erubescens* fossils from the Charleston Bump, *Univ Alabama McNair J*, 12, 19-40, 2012.
- 575 Braga-Henriques A., Carreiro-Silva M., Porteiro F.M., de Matos V., Sampaio I., Ocaña O., and Avila S.P.: The association between a deep-sea gastropod *Pedicularia sicula* and its coral host *Errina dabneyi* in the Azores. *ICES J. Mar. Sci.* 68: 399–407, <http://doi.org/10.1093/icesjms/fsq066>, 2010.

- Burke, A. and Robinson, L. F.: The Southern Ocean's Role in Carbon Exchange During the Last Deglaciation, *Science*, 335, 557–561, <https://doi.org/10.1126/science.1208163>, 2012.
- 580 Cairns, S. D.: A generic revision of the Stylasterina (Coelenterata: Hydrozoa). Part 1, Description of the genera, *B. Mar. Sci.*, 33, 427-508, 1983a.
- Cairns, S. D.: Antarctic and Subantarctic Stylasterina (Coelenterata: Hydrozoa), in: *Biology of the Antarctic Seas XIII*, vol. 38, edited by: Kornicker, S., American Geophysical Union, Washington, D. C., USA, 61–164, 1983b.
- 585 Cairns, S. D.: A generic revision of the Stylasteridae (Coelenterata: Hydrozoa). (Coelenterata: Hydrozoa). Part 3, Keys to the genera, *B. Mar. Sci.*, 49, 538-545, 1991.
- Cairns, S. D.: Worldwide distribution of the Stylasteridae (Cnidaria: Hydrozoa), *Sci. Mar.*, 56, 125–130, 1992.
- Cairns, S. D.: Global Diversity of the Stylasteridae (Cnidaria: Hydrozoa: Athecatae), *PLoS ONE*, 6, e21670, <https://doi.org/10.1371/journal.pone.0021670>, 2011.
- 590 Cairns, S. D. and Macintyre, I. G.: Phylogenetic Implications of Calcium Carbonate Mineralogy in the Stylasteridae (Cnidaria: Hydrozoa), *PALAIOS*, 7, 96-107, <https://doi.org/10.2307/3514799>, 1992.
- Chen, S., Gagnon, A. C., and Adkins, J. F.: Carbonic anhydrase, coral calcification and a new model of stable isotope vital effects, *Geochim. Cosmochim. Ac.*, 236, 179–197, <https://doi.org/10.1016/j.gca.2018.02.032>, 2018.
- Chen, T., Robinson, L. F., Burke, A., Claxton, L., Hain, M. P., Li, T., Rae, J. W. B., Stewart, J., Knowles, T. D. J., Fornari, D. J., and Harpp, K. S.: Persistently well-ventilated intermediate-depth ocean through the last deglaciation, *Nat. Geosci.*, 595 <https://doi.org/10.1038/s41561-020-0638-6>, 2020.
- Chong, A. K., and Stratford, P.: Underwater digital stereo-observation technique for red hydrocoral study. *Photogramm. Eng. Rem. S.*, 68(7), 745–752, 2002.
- Druffel, E. R. M.: Geochemistry of corals: Proxies of past ocean chemistry, ocean circulation, and climate, *P. Natl. Acad. Sci.*, 94, 8354–8361, <https://doi.org/10.1073/pnas.94.16.8354>, 1997.
- 600 Druffel, E. R. M., King, L. L., Belostock, R. A., and Buesseler, K. O.: Growth rate of a deep-sea coral using 210Pb and other isotopes, *Geochim. Cosmochim. Ac.*, 54, 1493–1499, [https://doi.org/10.1016/0016-7037\(90\)90174-J](https://doi.org/10.1016/0016-7037(90)90174-J), 1990.
- Emiliani, C.: Pleistocene temperatures, *J. Geol.*, 63, 538–578, <https://doi.org/10.1086/626295>, 1955.
- Emiliani, C., Hudson, J. H., Shinn, E. A., and George, R. Y.: Oxygen and carbon isotopic growth record in a reef coral from the Florida Keys and a deep-sea coral from Blake Plateau, *Science*, 202, 627–629, 605 <https://doi.org/10.1126/science.202.4368.627>, 1978.
- Epstein, S., Buchsbaum, R., Lowenstam, H., and Urey, H. C.: Carbonate-water isotopic temperature scale, *Geol. Soc. Am. Bull.*, 62, 417–426, [https://doi.org/10.1130/0016-7606\(1951\)62\[417:CITS\]2.0.CO;2](https://doi.org/10.1130/0016-7606(1951)62[417:CITS]2.0.CO;2), 1951.
- Epstein, S., Buchsbaum, R., Lowenstam, H., and Urey, H. C.: Revised carbonate-water isotopic temperature scale, *Bull. Geol. Soc. Am.*, 64, 1315–1326, [https://doi.org/10.1130/0016-7606\(1953\)64\[1315:RCITS\]2.0.CO;2](https://doi.org/10.1130/0016-7606(1953)64[1315:RCITS]2.0.CO;2), 1953.
- 610 Fallon, S. J., Thresher, R. E., and Adkins, J.: Age and growth of the cold-water scleractinian *Solenosmilia variabilis* and its reef on SW Pacific seamounts, *Coral Reefs*, 33, 31–38, <https://doi.org/10.1007/s00338-013-1097-y>, 2014.

- Gerrish, L., Fretwell, P., & Cooper, P., High resolution vector polylines of the Antarctic coastline (7.5), UK Polar Data Centre, Natural Environment Research Council, UK Research & Innovation [Basemap] <https://doi.org/10.5285/bc71347d-298a-4df3-88b0-cb9a908db166>, 2022.
- 615 Gladfelter, E. H.: Skeletal development in *Acropora cervicornis*: I. Patterns of calcium carbonate accretion in the axial corallite, *Coral Reefs*, 1, 45–51, <https://doi.org/10.1007/BF00286539>, 1982.
- Gladfelter, E. H.: Skeletal Development in *Acropora cervicornis*: II. Diel patterns of calcium carbonate accretion, *Coral Reefs*, 2, 91–100, <https://doi.org/10.1007/BF02395279>, 1983.
- 620 Gladfelter, E. H.: Skeletal Development in *Acropora cervicornis*: III. A comparison of monthly rates of linear extension and calcium carbonate accretion measured over a year, *Coral Reefs*, 3, 51–57, <https://doi.org/10.1007/BF00306140>, 1984.
- Gordon, A.: Calibrated Hydrographic Data acquired with a CTD in the Ross Sea during the Nathaniel B. Palmer expedition NBP0302 (2003), Interdisciplinary Earth Data Alliance [CTD/Rosette], <http://doi.org/10.1594/IEDA/317291>, 2016.
- Gordon, A. L., Orsi, A. H., Muench, R., Huber, B. A., Zambianchi, E., and Visbeck, M.: Western Ross Sea continental slope gravity currents, *Deep-Sea Res. Pt. II*, 56, 796–817, <https://doi.org/10.1016/j.dsr2.2008.10.037>, 2009.
- 625 Griffin, S. and Druffel, E. R. M.: Sources of Carbon to Deep-Sea Corals, *Radiocarbon*, 31, 533–543, <https://doi.org/10.1017/S0033822200012121>, 1989.
- Grossman, E. L. and Ku, T.-L.: Oxygen and carbon isotope fractionation in biogenic aragonite: temperature effects, *Chem. Geol. (Isotope Geoscience Section)*, 59, 59–74, [https://doi.org/10.1016/0168-9622\(86\)90057-6](https://doi.org/10.1016/0168-9622(86)90057-6), 1986.
- 630 Heikoop, J. M., Dunn, J. J., Risk, M. J., Schwarcz, H. P., McConnaughey, T. A., and Sandeman, I. M.: Separation of kinetic and metabolic isotope effects in carbon-13 records preserved in reef coral skeletons, *Geochim. Cosmochim. Ac.*, 64, 975–987, [https://doi.org/10.1016/S0016-7037\(99\)00363-4](https://doi.org/10.1016/S0016-7037(99)00363-4), 2000.
- Hill, T. M., Spero, H. J., Guilderson, T., LaVigne, M., Clague, D., Macalello, S., and Jang, N.: Temperature and vital effect controls on bamboo coral (*Isididae*) isotope geochemistry: A test of the “lines method”, *Geochem. Geophys. Geosy.*, 12, 14, <https://doi.org/10.1029/2010GC003443>, 2011.
- 635 Houlbrèque, F., Meibom, A., Cuif, J.-P., Stolarski, J., Marrocchi, Y., Ferrier-Pagès, C., Domart-Coulon, I., and Dunbar, R. B.: Strontium-86 labeling experiments show spatially heterogeneous skeletal formation in the scleractinian coral *Porites porites*, *Geophys. Res. Lett.*, 36, L04604, <https://doi.org/10.1029/2008GL036782>, 2009.
- Jacobs, S.: Calibrated Hydrographic Data from the Ross Sea acquired with a CTD during the Nathaniel B. Palmer expedition NBP0408 (2004), Interdisciplinary Earth Data Alliance [CTD/Rosette], <http://doi.org/10.1594/IEDA/307443>, 2015.
- 640 Jacobs, S. S., Fairbanks, R. G., and Horibe, Y. G.: Origin and evolution of water masses near the Antarctic continental margin: Evidence from H₂18O/H₂16O ratios in seawater, in: *Antarctic Research Series*, vol. 43, edited by: Jacobs, S., American Geophysical Union, Washington, D. C., 59–85, <https://doi.org/10.1029/AR043p0059>, 1985.
- Jacobs, S. S., Amos, A. F., and Bruchhausen, P. M.: Ross Sea oceanography and Antarctic Bottom Water formation, *Deep-Sea Res. and Oceanographic Abstracts*, 17, 935–962, [https://doi.org/10.1016/0011-7471\(70\)90046-X](https://doi.org/10.1016/0011-7471(70)90046-X), 1970.
- 645 Kershaw, J., Stewart, J. A., Strawson, I., de Carvalho Ferreira, M. L., Robinson, L. F., Hendry, K. R., Samperiz, A., Burk, A., Rae, J. W., Day, R. D., and Etnoyer, P. J.: Ba/Ca of stylasterid coral skeletons records dissolved seawater barium concentrations, *Chemical Geology*, 662, p. 121355, <https://doi.org/10.1016/j.chemgeo.2023.121355>, 2023.

- Kim, S. T., Mucci, A., and Taylor, B. E.: Phosphoric acid fractionation factors for calcite and aragonite between 25 and 75 °C: revisited, *Chemical Geology*, 246, 135-146, <https://doi.org/10.1016/j.chemgeo.2007.08.005>, 2007.
- 650 King, T. M., Rosenheim, B. E., Post, A. L., Gabris, T., Burt, T., and Domack, E. W.: Large-scale intrusion of circumpolar deep water on Antarctic margin recorded by stylasterid corals, *Paleoceanography and Paleoclimatology*, 33(11), 1306–1321, <http://doi.org/10.1029/2018PA003439>, 2018.
- Kurtz, D. D. and Bromwich, D. H.: A recurring, atmospherically forced polynya in Terra Nova Bay, in: *Oceanology of the Antarctic Continental Shelf*, vol. 43, edited by: Jacobs, S., American Geophysical Union, Washington, D. C., USA, 177–201, 1985.
- 655 Lécuyer, C., Hutzler, A., Amiot, R., Daux, V., Grosheny, D., Otero, O., Martineau, F., Fourel, F., Balter, V. and Reynard, B.: Carbon and oxygen isotope fractionations between aragonite and calcite of shells from modern molluscs, *Chemical Geology*, 332, pp. 92-101, <http://doi.org/10.1016/j.chemgeo.2012.08.034>, 2012.
- Matsuoka, K., Skoglund, A., Roth, G., de Pomereu, J., Griffiths, H., Headland, R., Herried, B., Katsumata, K., Le Brocq, A., Licht, K., Morgan, F., Neff, P. D., Ritz, C., Scheinert, M., Tamura, T., Van de Putte, A., van den Broeke, M., von Deschwandens, A., Deschamps-Berger, C., Van Liefferinge, B., Tronstad, S., and Melvær, Y.: Quantarctica, an integrated mapping environment for Antarctica, the Southern Ocean, and sub-Antarctic islands, *Environ. Modell. Softw.*, 140, 105015, <https://doi.org/10.1016/j.envsoft.2021.105015>, 2021.
- 660 McConnaughey, T.: ^{13}C and ^{18}O isotopic disequilibrium in biological carbonates: I. Patterns, *Geochim. Cosmochim. Ac.*, 53, 151-162, [https://doi.org/10.1016/0016-7037\(89\)90282-2](https://doi.org/10.1016/0016-7037(89)90282-2), 1989a.
- 665 McConnaughey, T.: ^{13}C and ^{18}O isotopic disequilibrium in biological carbonates II. In vitro simulation of kinetic isotope effects, *Geochim. Cosmochim. Ac.*, 53, 163–171, [https://doi.org/10.1016/0016-7037\(89\)90283-4](https://doi.org/10.1016/0016-7037(89)90283-4), 1989b.
- McCrea, J. M.: On the Isotopic Chemistry of Carbonates and a Paleotemperature Scale, *J. Chem. Phys.*, 18, 849–857, <https://doi.org/10.1063/1.1747785>, 1950.
- 670 Mikkelsen, N., Erlenkeuser, H., Killingley, J. S., and Berger, W. H.: Norwegian corals: radiocarbon and stable isotopes in *Lophelia pertusa*, *Boreas*, 11, 163–171, <https://doi.org/10.1111/j.1502-3885.1982.tb00534.x>, 2008.
- Miller, K. J., Mundy, C. N., and Chadderton, W. L.: Ecological and genetic evidence of the vulnerability of shallow-water populations of the stylasterid hydrocoral *Errina novaezelandiae* in New Zealand’s fiords. *Aquat. Conserv.*, 14(1), 75–94, <https://doi.org/10.1002/aqc.597>, 2004.
- 675 Moseley, H. N.: XIV. The Croonian lecture. —On the structure of the stylasteridæ, a family of the hydroid stony corals, *Phil. Trans. R. Soc.*, 169, 425–503, <https://doi.org/10.1098/rstl.1878.0014>, 1878.
- Mouginot, J., B. Scheuchl, and E. Rignot. 2017. MEaSURES Antarctic Boundaries for IPY 2007-2009 from Satellite Radar, Version 2 [Coastline and grounding line], Boulder, Colorado USA. NASA National Snow and Ice Data Center Distributed Active Archive Center, <http://dx.doi.org/10.5067/AXE4121732AD>, <https://nsidc.org/data/nsidc-0709/versions/2>, 2022.
- 680 O’Neil, J. R., Clayton, R. N., and Mayeda, T. K.: Oxygen Isotope Fractionation in Divalent Metal Carbonates, *J. Chem. Phys.*, 51, 5547–5558, <https://doi.org/10.1063/1.1671982>, 1969.
- Philipp, E., Brey, T., Pörtner, H.-O., and Abele, D.: Chronological and physiological ageing in a polar and a temperate mud clam, *Mech. Ageing Dev.*, 126, 598–609, <https://doi.org/10.1016/j.mad.2004.12.003>, 2005.

- 685 Pica, D., Cairns, S. D., Puce, S., and Newman, W. A.: Southern hemisphere deep-water stylasterid corals including a new species, *Errina labrosa* sp. n. (Cnidaria, Hydrozoa, Stylasteridae), with notes on some symbiotic scalpellids (Cirripedia, Thoracica, Scalpellidae), *ZooKeys*, (472), 1, <http://doi.org/10.3897/zookeys.472.8547>, 2015.
- Picco, P., Bergamasco, A., Demicheli, L., Manzella, G., Meloni, R., and Paschini, E.: Large-scale circulation features in the Central and Western Ross Sea (Antarctica), in: *Ross Sea Ecology*, Springer, Berlin, Heidelberg, Germany, 95–105, 2000.
- 690 Puce, S., Tazioli, S., and Bavestrello, G.: First evidence of a specific association between a stylasterid coral (Cnidaria: Hydrozoa: Stylasteridae) and a boring cyanobacterium, *Coral Reefs*, 28, 177–177, <https://doi.org/10.1007/s00338-008-0411-6>, 2009.
- Puce, S., Pica, D., Mancini, L., Brun, F., Peverelli, A., and Bavestrello, G.: Three-dimensional analysis of the canal network of an Indonesian Stylaster (Cnidaria, Hydrozoa, Stylasteridae) by means of X-ray computed microtomography. *Zoomorphology* 130, 85–95, <https://doi.org/10.1007/s00435-011-0120-5>, 2011.
- 695 Ralph, R. and Maxwell, J. G. H.: Growth of two Antarctic lamellibranchs: *Adamussium colbecki* and *Laternula elliptica*, *Mar. Biol.*, 42, 171–175, <https://doi.org/10.1007/BF00391569>, 1977.
- Risk, M. J., Heikoop, J. M., Snow, M. G., and Beukens, R.: Lifespans and growth patterns of two deep-sea corals: *Primnoa resedaeformis* and *Desmophyllum cristagalli*, *Hydrobiologia*, 471, 125–131, <https://doi.org/10.1023/A:1016557405185>, 2002.
- 700 Robinson, L. F. and van de Flierdt, T.: Southern Ocean evidence for reduced export of North Atlantic Deep Water during Heinrich event 1, *Geology*, 37, 195–198, <https://doi.org/10.1130/G25363A.1>, 2009.
- Robinson, L. F., Adkins, J., Keigwin, L. D., Southon, J., Fernandez, D. P., Wang, S.-L., and Scheirer, D. S.: Radiocarbon variability in the Western North Atlantic during the Last Deglaciation, *Science*, 310, 1469–1473, <https://doi.org/10.1126/science.1114832>, 2005.
- 705 Robinson, L. F., Adkins, J. F., Frank, N., Gagnon, A. C., Prouty, N. G., Brendan Roark, E., and de Flierdt, T. van: The geochemistry of deep-sea coral skeletons: A review of vital effects and applications for palaeoceanography, *Deep-Sea Res. Pt. II: Topical Studies in Oceanography*, 99, 184–198, <https://doi.org/10.1016/j.dsr2.2013.06.005>, 2014.
- Romanek, C. S., Grossman, E. L., and Morse, J. W.: Carbon isotopic fractionation in synthetic aragonite and calcite: Effects of temperature and precipitation rate, *Geochim. Cosmochim. Ac.*, 56, 419–430, [https://doi.org/10.1016/0016-7037\(92\)90142-6](https://doi.org/10.1016/0016-7037(92)90142-6), 1992.
- 710 Román-González, A., Scourse, J. D., Butler, P. G., Reynolds, D. J., Richardson, C. A., Peck, L. S., Brey, T., and Hall, I. R.: Analysis of ontogenetic growth trends in two marine Antarctic bivalves *Yoldia eightsi* and *Laternula elliptica*: Implications for sclerochronology, *Palaeogeogr. Palaeoecol.*, 465, 300–306, <https://doi.org/10.1016/j.palaeo.2016.05.004>, 2017.
- 715 Samperiz, A., Robinson, L. F., Stewart, J. A., Strawson, I., Leng, M. J., Rosenheim, B. E., Ciscato, E. R., Hendry, K. R., and Santodomingo, N.: Stylasterid corals: A new paleotemperature archive, *Earth Planet. Sc. Lett.*, 545, 116407, <https://doi.org/10.1016/j.epsl.2020.116407>, 2020.
- Sandrini, S., Ait-Ameur, N., Rivaro, P., Massolo, S., Touratier, F., Tositti, L., and Goyet, C.: Anthropogenic carbon distribution in the Ross Sea, Antarctica, *Antarct. Sci.*, 19, 395–407, <https://doi.org/10.1017/S0954102007000405>, 2007.
- Shackleton, N.: Oxygen isotope analyses and Pleistocene temperatures re-assessed, *Nature*, 215, 15–17, <https://doi.org/10.1038/215015a0>, 1967.

- 720 Smith, J. E., Schwarcz, H. P., Risk, M. J., McConnaughey, T. A., and Keller, N.: Paleotemperatures from deep-sea corals: overcoming ‘vital effects,’ *PALAIOS*, 15, 25–32, 2000.
- Smith, J. E., Schwarcz, H. P., and Risk, M. J.: Patterns of isotopic disequilibria in azooxanthellate coral skeletons, *Hydrobiologia*, 471, 111–115, <https://doi.org/10.1023/A:1016553304276>, 2002.
- 725 Stewart, J.A., Robinson, L.F., Day, R.D., Strawson, I., Burke, A., Rae, J.W., Spooner, P.T., Samperiz, A., Etnoyer, P.J., Williams, B., Paytan, A., Leng, M.J., Häussermann, V., Wickes, L.N., Bratt, R., and Pryer, H.: Refining trace metal temperature proxies in cold-water scleractinian and stylasterid corals, *Earth Planet. Sc. Lett.*, 545, p.116412, <http://doi.org/10.1016/j.epsl.2020.116412>, 2020.
- Stewart, J. A., Strawson, I., Kershaw, J., and Robinson, L. F.: Stylasterid corals build aragonite skeletons in undersaturated water despite low pH at the site of calcification, *Sci Rep*, 12, 13105, <https://doi.org/10.1038/s41598-022-16787-y>, 2022.
- 730 Stratford, P., Stewart, B. G., and Chong, A.: In situ growth rate measurements on the red hydrocoral, *Errina novaezelandiae*, in Doubtful Sound, New Zealand fjords: Researching, managing, and conserving a unique ecosystem, *New Zeal. J. Mar. Fresh.*, 35(4), 653–661. <https://doi.org/10.1080/00288330.2001.9517032>, 2001.
- Swart, P. K.: Carbon and oxygen isotope fractionation in scleractinian corals: a review, *Earth-Sci. Rev.*, 19, 51–80, [https://doi.org/10.1016/0012-8252\(83\)90076-4](https://doi.org/10.1016/0012-8252(83)90076-4), 1983.
- 735 Thresher, R., Tilbrook, B., Fallon, S., Wilson, N., and Adkins, J.: Effects of chronic low carbonate saturation levels on the distribution, growth and skeletal chemistry of deep-sea corals and other seamount megabenthos, *Mar. Ecol. Prog. Ser.*, 442, 87–99, <https://doi.org/10.3354/meps09400>, 2011.
- Urey, H. C.: The thermodynamic properties of isotopic substances, *J. Chem. Soc. (Resumed)*, 562–581, <https://doi.org/10.1039/jr9470000562>, 1947.
- 740 Urushihara, Y., Hasegawa, H., and Iwasaki, N.: X-ray micro-CT observation of the apical skeleton of Japanese white coral *Corallium konojoi*, *J. Exp. Mar. Biol. Ecol.*, 475, 124–128, <https://doi.org/10.1016/j.jembe.2015.11.016>, 2016.
- Visbeck, M.: Calibrated Hydrographic Data from the Ross Sea acquired with a CTD during the Nathaniel B. Palmer expedition NBP0402 (2004), Interdisciplinary Earth Data Alliance [CTD/Rosette], <http://doi.org/10.1594/IEDA/307431>, 2015.
- 745 Weber, J. N.: Deep-sea ahermatypic scleractinian corals: isotopic composition of the skeleton, *Deep-Sea Res. and Oceanographic Abstracts*, 20, 901–909, [https://doi.org/10.1016/0011-7471\(73\)90108-3](https://doi.org/10.1016/0011-7471(73)90108-3), 1973.
- Weber, J. N. and Woodhead, P. M. J.: Carbon and oxygen isotope fractionation in the skeletal carbonate of reef-building corals, *Chem. Geol.*, 6, 93–117, [https://doi.org/10.1016/0009-2541\(70\)90009-4](https://doi.org/10.1016/0009-2541(70)90009-4), 1970.
- Weber, J. N. and Woodhead, P. M. J.: Stable isotope ratio variations in non-scleractinian coelenterate carbonates as a function of temperature, *Mar. Biol.*, 15, 293–297, <https://doi.org/10.1007/BF00401388>, 1972.
- 750 Wisshak, M., López Correa, M., Zibrowius, H., Jakobsen, J., and Freiwald, A.: Skeletal reorganisation affects geochemical signals, exemplified in the stylasterid hydrocoral *Errina dabneyi* (Azores Archipelago), *Mar. Ecol. Prog. Ser.*, 397, 197–208, <https://doi.org/10.3354/meps08165>, 2009.
- Wisshak, M., Form, A., Jakobsen, J., and Freiwald, A.: Temperate carbonate cycling and water mass properties from intertidal to bathyal depths (Azores), *Biogeosciences*, 7, 2379–2396, <https://doi.org/10.5194/bg-7-2379-2010>, 2010.

755 WOCE Hydrographic Programme, WHP: Hydrochemistry measured on water bottle samples during Akademik Ioffe cruise 90KDIOFFE6_1 on section S04P, PANGAEA [CTD/Rosette], <https://doi.org/10.1594/PANGAEA.837058>, 2002.